# A new predictive multi-zone model for HCCI engine combustion

**Bissoli, M.[a], Frassoldati, A.[a], Cuoci, A.[a], Ranzi, E.[a], Mehl, M.[b], Faravelli, T.[a]***

[a] Department of Chemistry, Materials and Chemical Engineering "G. Natta", Politecnico di Milano, Piazza Leonardo da Vinci 32, 20133 Milan, Italy

[b] Lawrence Livermore National Laboratory, 7000 East Avenue, 94550 Livermore (CA), USA

---

**Author 1**
Mattia Bissoli
*Dipartimento di Chimica, Materiali e Ingegneria Chimica "G. Natta"*
*Politecnico di Milano*
*P.zza Leonardo da Vinci 32, 20133 Milano - ITALY*
Phone: (039) 0223993243
Email: mattia.bissoli@polimi.it

**Author 2**
Alessio Frassoldati
*Dipartimento di Chimica, Materiali e Ingegneria Chimica "G. Natta"*
*Politecnico di Milano*
*P.zza Leonardo da Vinci 32, 20133 Milano - ITALY*
Phone: (039) 0223993286
Email: alessio.frassoldati@polimi.it

**Author 3**
Alberto Cuoci
*Dipartimento di Chimica, Materiali e Ingegneria Chimica "G. Natta"*
*Politecnico di Milano*
*P.zza Leonardo da Vinci 32, 20133 Milano - ITALY*
Phone: (039) 0223993283
Email: alberto.cuoci@polimi.it

**Author 4**
Eliseo Ranzi
*Dipartimento di Chimica, Materiali e Ingegneria Chimica "G. Natta"*
*Politecnico di Milano*
*P. zza Leonardo da Vinci 32, 20133 Milano - ITALY*
Phone: (039) 0223993250
Email: eliseo.ranzi@polimi.it

**Author 5**
Marco Mehl
*Materials Science Division*
*Lawrence Livermore National Laboratory*
*7000 East Avenue, 94550 Livermore (CA) - USA*
Phone: (01) 9254236993
Email: mehl6@llnl.gov

**Author 6**
Tiziano Faravelli
*Dipartimento di Chimica, Materiali e Ingegneria Chimica "G. Natta"*
*Politecnico di Milano*
*P.zza Leonardo da Vinci 32, 20133 Milano - ITALY*
Phone: (039) 0223993282
Email: tiziano.faravelli@polimi.it

***Corresponding Author:**
Tiziano Faravelli
*Dipartimento di Chimica, Materiali e Ingegneria Chimica "G. Natta"*
*Politecnico di Milano*
*P.zza Leonardo da Vinci 32, 20133 Milano - ITALY*
Phone: (039) 0223993282
Email: tiziano.faravelli@polimi.it

---

## Abstract

This work introduces a new predictive multi-zone model for the description of combustion in Homogeneous Charge Compression Ignition (HCCI) engines. The model exploits the existing OpenSMOKE++ computational suite to handle detailed kinetic mechanisms, providing reliable predictions of the in-cylinder auto-ignition processes. All the elements with a significant impact on the combustion performances and emissions, like turbulence, heat and mass exchanges, crevices, residual burned gases, thermal and feed stratification are taken into account. Compared to other computational approaches, this model improves the description of mixture stratification phenomena by coupling a wall heat transfer model derived from CFD application with a proper turbulence model. Furthermore, the calibration of this multi-zone model requires only three parameters, which can be derived from a non-reactive CFD simulation: these adaptive variables depend only on the engine geometry and remain fixed across a wide range of operating conditions, allowing the prediction of auto-ignition, pressure traces and pollutants. This computational framework enables the use of detail kinetic mechanisms, as well as Rate of Production Analysis (RoPA) and Sensitivity Analysis (SA) to investigate the complex chemistry involved in the auto-ignition and the pollutants formation processes. In the final sections of the paper, these capabilities are demonstrated through the comparison with experimental data.



**Keywords:** HCCI engine; Multi-zone model; Kinetic analyses

# Nomenclature

**Latin Symbols**

| | |
|---|---|
| $A$ | External area [$m^2$] |
| $C$ | Engine Compression Ratio |
| $C_p$ | Zone Constant-Pressure Specific Heat [J/kg/K] |
| $Cu_w$ | Engine specific parameter for the wall function model |
| $Cu_z$ | Engine specific parameter for the turbulence model |
| $C_x$ | Coefficient for the convective flux between crevice and outer zone [$kg/s/Pa^{0.5}$] |
| $D$ | Zone diameter [m] |
| $\mathcal{D}$ | Diffusion coefficient [$m^2/s$] |
| $d$ | Zone thickness [m] |
| $G$ | G variable [Pa × $m^3$] |
| $H$ | Zone height [m] |
| $h$ | Specific enthalpy [J/kg] |
| $J$ | Specific diffusive mass flux [$kg/m^2/s$] |
| $\mathcal{K}$ | Von Kärmän constant (0.41) |
| $L_A$ | Crank-arm radius [m] |
| $L_C$ | Connecting rod length [m] |
| $m$ | Mass [kg] |
| $\dot{m}$ | Mass flow rate [km/s] |
| $MW$ | Molecular weight [kg/kmol] |
| $NE$ | Total number of unknowns/equations |
| $NP$ | Total number of parameters |
| $NR$ | Total number of reactions |
| $NS$ | Total number of species |
| $NZ$ | Total number of zones |
| $P$ | Pressure [Pa] |

| | |
|---|---|
| $Pr$ | Prandtl number |
| $\dot{Q}$ | Heat [J/s] |
| $R$ | Ideal gas constant [J/kmol/K] |
| $r^+$ | Dimensionless distance in the normal direction |
| $Sc$ | Schmidt number |
| $S_{crev}$ | Gap size of the top land crevice [m] |
| $\langle S_P \rangle$ | Mean piston speed [m/s] |
| $s$ | Sensitivity coefficient |
| $\tilde{s}$ | Normalized sensitivity coefficient |
| $t$ | Time [s] |
| $T$ | Temperature [K] |
| $T^+$ | Dimensionless temperature profile |
| $u$ | Specific internal energy [J/kg] |
| $u^*$ | Friction velocity [m/s] |
| $V$ | Volume [$m^3$] |
| $V_{clearance}$ | Clearance volume [$m^3$] |
| $w$ | Weights for mass fluxes evaluation |
| $x$ | Molar fraction |
| $y$ | System unknowns |
| $y^+$ | Dimensionless distance from the cylinder wall |

**Greek Symbols**

| | |
|---|---|
| $\alpha$ | Constant of the turbulence model (0.06) |
| $\beta$ | Ratio Between the cylinder diameter and the instantaneous cylinder height |

| | |
|---|---|
| $\gamma$ | Constant-pressure and constant-volume specific heat ratio |
| $\theta$ | Crank Angle (CA) [deg] |
| $\lambda$ | Thermal conductivity [W/m/K] |
| $\mu$ | Dynamic viscosity [Pa × s] |
| $\dot{\Omega}$ | Formation rates [kmol/m$^3$s] |
| $\rho$ | Density [kg/m$^3$] |
| $\omega$ | Mass Fraction |
| $\nu$ | Kinematic viscosity [m$^2$/s] |

**Superscripts**

| | |
|---|---|
| $\widehat{\ }$ | Mass-based |
| $BDC$ | Bottom Dead Center |
| $L$ | Laminar |
| $T$ | Turbulent |
| $TDC$ | Top Dead Center |

**Subscripts**

| | |
|---|---|
| $atm$ | Atmospheric |
| $cyl$ | Cylinder properties |
| $cond$ | Conductive |
| $crev$ | Crevice |
| $diff$ | Diffusive |
| $end$ | End cycle |
| $i$ | Species index |
| $k$ | Zone Index |
| $n$ | Normal direction |
| $wall$ | Wall properties |

# 1 Introduction

The increasing demand of fuel-efficient engines and the increasingly strict environmental regulations are pushing powertrain designs towards new combustion strategies. Among these, the use of a highly lean premixed charge ignited by compression guarantees to Homogeneous Charge Compression Ignition (HCCI) engines the capability of virtually nullify NOx, PAH and soot emissions, thanks to the simultaneous ignition in multiple sites of the mixture without flame propagation [1,2]. This, coupled with the high thermal and combustion efficiency, makes HCCI a promising alternative to conventional internal combustion (IC) engines, even though several challenges still need to be addressed [3,4]. Differently from traditional Spark Ignition (SI) engines, where the fuel is ignited by a spark, or Direct Injection (DI) Compression Ignition (CI) engines, where fuel injection controls the onset of combustion, the combustion timing in HCCI systems is kinetically controlled. Moreover, the Rate of Heat Release (HRR) is typically much higher than the one observed in SI and DI, where the combustion rate depends on the flame propagation speed or the injection duration. In HCCI engines, the ignition event strongly depends on the fuel quality, the initial conditions of the charge at valve closure and on the thermodynamic history experienced during compression. In order to mitigate these shortcomings, HCCI engines usually operate under lean conditions, resulting in higher emissions of partial combustion products (like CO and HC) and reduced high-loads limit. Nevertheless, the environmental advantages of HCCI are further emphasized by recent experimental works feeding HCCI engines with biofuels [5,6].

In an effort to understand the operability limits of the HCCI engine, several researchers investigated the role of fuel composition, engine geometry and in-cylinder conditions on the engine performances and emissions [7-12]. Mathematical models also represent a very useful resource, thanks to the possibility to decouple physical phenomena. Computational Fluid Dynamics (CFD) tools provide a detailed description of the flows and transport phenomena occurring in the system,

adopting simplified or skeletal kinetic mechanisms in order to limit the already high computational effort. At the other end of the spectrum, the so-called “zone models” rely on a simplified description of the fluid dynamics and transport phenomena in order to focus more on chemical kinetics, by means of detailed mechanisms [13]. Scientific literature has been demonstrated that HCCI combustion is mainly controlled by chemical kinetics and less affected by fluid dynamics [14], highlighting the need of effective predictive models able to handle detailed chemistry and to investigate the effect of operating conditions on the engine performances.

Thanks to their characteristics, zone models have the potential to reach these targets. From an historical point of view, zone models can be classified into two main categories. “Single-zone” models treat the in-cylinder volume as a single homogeneous well-mixed reactor with time-variable volume [14-16]. This modeling approach has negligible computational costs, but local temperature and composition inhomogeneities are ignored, leading to an under prediction of the combustion duration and an over-prediction of the Pressure Rise Rate (PRR) [16]. “Multi-Zone” models aim to overcome these limitations by splitting the cylinder volume into several domains called zones, each of which treated as a well-mixed reactor with its own dynamics is terms of temperature and composition. All the multi-zone models reported in literature are based on these assumptions and mainly differ on how these zones interact.

“Balloon-type” multi-zone models consider the zone as a deformable, fixed-mass control volume. Heat and/or mass fluxes among zones are usually neglected, while temperature stratification is accounted for by means of different exchange level of the zones with the walls. Total heat loss is calculated using empirical correlations [17-19], and the pressure is assumed uniform over the entire domain at each simulation step. Andreatta [20] developed one of the first “balloon-type” models, where zones exchange mass at a prescribed rate and lose heat with the cylinder walls on the basis of their temperature rather than on the average cylinder temperature, and the total heat flux is

calculated by means of the Woschni [17] correlation. Easley et al. [21] described the HCCI combustion in terms of crevice, boundary layer, outer and inner (adiabatic) core regions, using a model where mass exchanges were allowed (except for the inner core) in order to maintain uniform pressure. Noda and Foster [22] focused their attention on the strategies to control combustion duration in hydrogen-fueled HCCI engines. With their model, they demonstrated that combustion duration is affected more by thermal stratification rather than fuel stratification. Fiveland and Assanis [23] developed a two-zone model while Ogink and Golovitchev [24] a model similar to the Easley's one but coupled with a cycle simulation software. Xu et al. [25] highlighted the advantages of the multi-zone approaches compared to the single zone ones. Orlandini et al. [26] also developed a balloon-type model. Kodavasal et al. [27] developed a balloon-type multi-zone model where zones do not exchange mass or heat among each other, but they exchange heat with the cylinder walls based on weights obtained from CFD calculations. Mehl et al. [28] developed a multi-zone model based on the idea of a boundary layer involved in the thermal interaction with the cylinder walls and an adiabatic core. Initial conditions were estimated on the basis of 1-D simulations in order to provide the correct boundary conditions of temperature, pressure, internal EGR and chemical composition. Also Kozarac et al. [29] developed a six-zone model where consistent initial and boundary conditions are provided by a 1-D cycle simulation software in order to evaluate.

"Onion-skin" models discretize the reactive volume into concentric cylinders, assuming that the thermal stratification before the auto-ignition is mainly controlled by the heat exchanged with the walls. Transport equations are not explicitly solved and neighboring zones exchange heat and mass based on simplified turbulent sub-models. Only the external and the crevice (if present) zones exchange heat with the cylinder walls. Komninos et al. [30] developed an onion-like model based on constant thickness zones, where the heat loss is evaluated with the Annand [18] correlation. In a recent publication, Komninos and Kosmadakis [31] implemented a custom heat transfer model

based on the zone temperature instead of the average cylinder temperature. Kongsereeparp and Checkel [32] and Guo et al. [33] also developed similar onion-skin models.

Another possible approach is the multi-zone modeling based on Probability Density Functions (PDFs), where the system is solved in the composition space instead of the physical space. Kraft et al. [34] and Maigaard et al. [35] give some examples of this method. Pitsch et al. [36] also developed a PDF-based model using the Representative Interactive Flamelet [36].

Multi-zone models are also coupled with CFD simulations. Aceves et al. [37-39] and Babajimopoulos et al. [40] used the CFD to define the thermal stratification up to a certain point during the compression stroke, in order to initialize the zones of the balloon-type multi-zone model adopted for the chemical kinetics description during the remaining part of the engine cycle.

Flowers et al. [41], Shi et al. [42], Felsch et al. [43], Kodavasal et al. [44] and Felsch et al. [45] further contribute to apply the multi-zone concepts to the HCCI modeling.

It is important to notice that most of the aforementioned multi-zone models use empirical correlations for predicting the heat exchanged with the boundaries based on experimental data not relevant to HCCI operations [46].

The main goal of this work is to provide a predictive tool able to investigate the effect of operating conditions on HCCI combustion performances and emissions using detailed chemistry and by taking into account all the elements with a significant impact on these aspects (such as turbulence, heat and mass exchanges, crevices, residual burned gases, thermal and feed stratification). A novel wall heat transfer model, derived from CFD applications, coupled with a proper turbulence model allows describing the mixture stratification deriving from boundary interactions and in-cylinder fluid motions. The ability of handling detailed kinetic mechanisms enables predictive fuel chemistry and pollutant formation calculations. Lastly, advanced kinetic tools like Rate of Production Analysis

(RoPA) and Sensitivity Analysis (SA) are implemented in order to investigate the complex chemistry controlling the auto-ignition mechanism and pollutants formation in different operating conditions.

# 2 The Multi-Zone Model

The model here presented follows the “Onion-skin” approach and represents a further evolution of an earlier version by Bissoli et al. [47]. The focus is on combustion, so only the compression and expansion phases of a four-stroke cycle are described. The model neglects valve dynamics effects, while gas flow to and from the crevices are accounted for. The simulation cycle starts at Intake Valve Closing (IVC) and ends at Exhaust Valve Opening (EVO). During the whole simulation, the model accounts for the chemistry, heat and mass exchange between adjacent zones, working both in single and multi-zone configurations. Neighboring zones can interact through work, heat and mass diffusion at interfaces (both laminar and turbulent). If the user requests multiple simulation cycles, a sub-model evaluates the characteristics of the Residual Burned Gases (RBG) after the discharging phase and the consistent initial conditions for the new cycle, assuming a complete and adiabatic mixing between the RBG remaining trapped in the cylinder and the fresh charge. The model easily manages detailed kinetic mechanisms and allows performing kinetic investigation by means of Rate of Production (ROPA) and Sensitivity Analysis (SA), in order to identify the effects of different engine parameters (i.e. compression ratio, engine speed, heat exchange) on the pathways controlling auto-ignition and leading to pollutant formation.

The mathematical formulation derives from different assumptions. First, in-cylinder mixture is described as an ideal gas. Pressure is assumed uniform inside the cylinder, except for crevices. The spatial discretization of the in-cylinder volume is carried out by considering each zone as an ideal reactor with time-variable volume and uniform temperature and composition. Crevices are described as a constant-volume variable-mass zone, characterized by a small pressure difference

with respect to the other sub-domains. This pressure difference defines a mass flux at the crevice/external zone interface. External zone and the crevices are also responsible for the interaction with the cylinder walls and the piston head. The inclusion of mass and heat exchange between zones improves the description of HCCI combustion, allowing thermal and composition stratification in the charge. In fact, the lack of an external device able to adjust the ignition timing makes stratification very important in controlling the combustion process. Initial in-cylinder temperature and composition distribution can be set as uniform or non-uniform according to a prescribed distribution (see paragraph 4.1.5).

## *2.1 Geometry and zone configuration*

As mentioned above, the zone configuration follows an onion-like structure (Figure 1). Zones can be initialized with the same volume or by specifying a different volume for each one. The crevice zone is defined based on the engine geometry.

The inner zone is identified as the core, while crevices are modeled as a ring-pack crevice with an equivalent surface/volume ratio, in order maintain the original cooling effect. The time variation of the total in-cylinder volume $V_{cyl}$ is obtained from the typical piston motion law [48]:

$$\frac{d\left(V_{cyl}/V_{clearance}\right)}{dt} = \frac{d\theta}{dt}\left(\frac{C-1}{2}\right) sin\,\theta \left[1 + \frac{cos\,\theta}{\sqrt{(L_C/L_A)^2 - sin^2\,\theta}}\right] \qquad (1)$$

where $\theta$ is the crank angle, $C$ the compression ratio and $L_C/L_A$ the ratio between the connecting rod length and the crank-arm radius. The geometry of each zone is evaluated at any time from its volume assuming that the ratio $\beta$ between its diameter and height is constant, and equal to the ratio between the cylinder diameter and the instantaneous cylinder height:

$$\frac{D_k}{H_k} = \frac{D_{cyl}}{H_{cyl}} = \beta \qquad k = 2, \dots, NZ \qquad (2)$$

Consequently, all the zones have the same shape, but their thickness varies during the cycle. Equation (2) provides the instantaneous height of the $k^{th}$ zone, while its diameter can be calculated as:

$$D_k = \sqrt[3]{\left(D_{cyl}\right)^3 - \frac{4\beta V_{k-1}}{\pi}} \qquad k = 2, \dots, NZ \qquad (3)$$

## *2.2 Model equations*

The mass of each zone is obtained by solving the following balance equation:

$$\frac{\partial m_k}{\partial t} = \dot{m}_k^{in} - \dot{m}_k^{out} \qquad k = 1, \dots, NZ \qquad (4)$$

where $\dot{m}_k^{in}$ and $\dot{m}_k^{out}$ represent mass fluxes entering and leaving the $k^{th}$ zone induced by the crevices (see section 2.6).

Similarly, the composition of each zone is evaluated from the species balance equation:

$$\frac{dm_{i,k}}{dt} = \dot{m}_{i,k}^{in} - \dot{m}_{i,k}^{out} - J_{i,k}A_k + \dot{\Omega}_{i,k}MW_iV_k \qquad \begin{matrix} k = 1, \dots, NZ \\ i = 1, \dots, NS \end{matrix} \qquad (5)$$

$J_{i,k}$ represents the net diffusive flux of species $i$ to the $k^{th}$ zone, and includes both laminar and turbulent contributions:

$$J_{i,k} = J_{i,k}^L + J_k^T = -\rho_k\left(\mathcal{D}_{i,k}^L + \mathcal{D}_k^T\right)\nabla\omega_{i,k} \qquad (6)$$

$\nabla\omega_{i,k}$ is the mass fraction gradient of species $i$ at the generic $k^{th}$ interface (Figure 1). The laminar mixture-averaged molar-base diffusion coefficient $\mathcal{D}_{i,k}^L$ is evaluated from the kinetic theory of gases and by properly averaging the binary diffusion coefficients on the mixture composition [49]. The turbulent diffusion coefficient $\mathcal{D}_k^T$, which is the same for all the species in the same zone, is evaluated using the turbulent viscosity $\mu^T$:

$$\mathcal{D}_k^T = \frac{\mu_k^T}{Sc^T \rho_k} \tag{7}$$

where $\mu^T$ is obtained from a proper sub-model described in section 2.3.

Temperature of the $k^{th}$ zone is evaluated by solving the energy balance:

$$m_k \frac{\partial \hat{u}_k}{\partial t} = \dot{m}_k^{in}\left(\hat{h}_k^{in} - \hat{h}_k\right) - P_k \frac{\partial V_k}{\partial t} + \dot{Q}_{k,diff} + \dot{Q}_{k,cond} - \dot{Q}_{k,wall} \tag{8}$$

The heat exchanged with neighboring zones $\dot{Q}_{k,cond}$, similarly to the mass diffusion, is calculated for each interface as follows:

$$\dot{Q}_{k,cond} = \lambda_{tot,k} A_k \nabla T \tag{9}$$

$$\lambda_{tot,k} = \lambda_k^L + \lambda_k^T \tag{10}$$

As for the mass diffusion coefficient, the laminar thermal conductivity of the zone is calculated from the pure species properties using proper mixture averaging rules [50]. Again, the turbulent contribution is function of the turbulent viscosity:

$$\lambda_k^T = \frac{C_{P_k} \mu_k^T}{Pr^T} \tag{11}$$

Lastly, $\dot{Q}_{k,wall}$ is null for all the zones but the most external one and the crevice zone. The model adopted for the evaluation of this term will be discussed in detail in section 2.4.

Equation (1) describes the rate of change of the total in-cylinder volume as a function of time, but no information regarding the rate of change of the individual zone volumes is given. To evaluate this, a new variable $G$ [51] is introduced, which can be considered a sort of pressure-weighted accumulated volume:

$$G_1 = 0 \tag{12}$$

$$G_k = \sum_{j=2}^{k} P_j V_j = \sum_{j=2}^{k} \frac{m_j}{MW_j} R T_j \qquad k = 2, \dots, NZ \tag{13}$$

Since $G$ couples pressure and volume, for obtaining the zone pressure it is necessary to solve a further equation for each zone. By assuming that pressure is the same in all the zones (except for the crevices), it is possible to write:

$$P_1 = \frac{m_1 R T_1}{MW_1 V_1} \tag{14}$$

$$P_k = P_{k-1} \qquad k = 2, \dots, NZ \tag{15}$$

Crevices pressure is calculated using the ideal gas law and differs from the pressure of the other zones as better discussed in section 2.6. For all the other zones, $P$ is calculated starting from the inner zone by taking into account the constraint on the total volume, and exploiting the $G$ definition:

$$P_{NZ} = \frac{G_{NZ}}{V_{cyl}} \tag{16}$$

$$V_{cyl} = \sum_{k=2}^{NZ} V_k \tag{17}$$

where $V_{cyl}$ is obtained from Equation (1). The volume of each zone $k$ (which is not a primitive variable) is then calculated as follow:

$$V_k = \frac{G_k - G_{k-1}}{P_k} \qquad k = 2, \dots, NZ \tag{18}$$

Using the $G$ variable instead of directly solving the zone volumes leads to a block tri-diagonal sparsity pattern of the Jacobian matrix associated with the multi-zone problem, allowing the use of more efficient solvers for stiff systems [52,53]. Globally, the model solves Equations (4)-(5), (8) and (12)-(16), leading to a Differential-Algebraic system (DAE) consisting of $NE = NZ \times (NS + 4)$ equations.

## *2.3 Turbulence and transport properties*

Turbulence plays a very important role in the thermal and compositional stratification inside the cylinder. Since stratification affects the combustion dynamics of HCCI engines, a proper model is

required. As already mentioned, the solution here adopted is based on the introduction of the turbulent viscosity $\mu^T$ as reference variable for the turbulence. The turbulent viscosity is estimated using the approach suggested by Yang and Martin [54], which has been successfully used in other multi-zones models [30,33]. According to this approach, $\mu^T$ is evaluated through a combination of two different empirical expressions for estimating the ratio $\frac{\mu^T}{\mu^L}$ (one proposed by Reichardt [55] and the other from Mellor [56]), in order to obtain an analytical solution of a 1-D energy equation. Equation 19 shows the final formulation obtained by Yang and Martin:

$$\frac{\mu_k^T}{\mu_k^L} = \mathcal{K} r_{n,k}^+ \left[1 - exp\left(-2\alpha\mathcal{K} r_{n,k}^+\right)\right] \tag{19}$$

$\mathcal{K} = 0.41$ and $\alpha = 0.06$ are respectively the von Karman constant and an adaptive parameter, defined by the authors in order to fit the trends corresponding to the two aforementioned correlations of Reichardt [55] and Mellor [56]. $r_{n,k}^+$ is a dimensionless distance from the cylinder walls, evaluated in the normal direction to the surface considered:

$$r_{n,k}^+ = \frac{u^*}{\mu_{wall}^L} \int_0^{r_n} \rho dr_n \tag{20}$$

where $\mu_{wall}^L$ is the laminar viscosity at wall, and $u^*$ is the friction velocity, a parameter related to the shear stress at the boundaries. The friction velocity is considered proportional to the mean piston speed [30,54] through an engine-specific constant $Cu_z$:

$$u^* = Cu_z \langle S_p \rangle \tag{21}$$

$Cu_z$ is an engine-specific parameter which is estimated using a non-reactive CFD calculation performed with the Lib-ICE libraries [57], a set of libraries and solvers specifically tailored for engine simulations that runs under the open-source CFD technology OpenFOAM®. Thanks to these libraries, it is possible to handle complex geometries with moving meshes, and to describe heat transfer with boundaries and combustion phenomena inside the cylinder. The procedure adopted for the definition of $Cu_z$ will be discussed in paragraph 2.7.1.

## 2.4 Wall heat transfer

Similarly to turbulence, wall heat transfer affects the thermal stratification inside the cylinder and the combustion behavior of HCCI engines. In order to provide a reliable prediction of the interaction with the boundaries, the present multi-zone model adopts a wall-function model for evaluating the heat exchanged with the cylinder walls and the piston surface. Here, the model proposed by Han and Reitz [58] has been adopted. The model derives from a simplified solution of a 1-D energy equation in the near-wall region:

$$\dot{Q}_{wall} = \frac{\rho C_p u^*_{wall} T ln(T/T_{wall})}{T^+} A \tag{22}$$

where $T^+$ is a dimensionless temperature profile defined as [58]:

$$T^+ = \int_0^{40} \frac{1}{\frac{1}{Pr} + 0.1 + 0.025y^+ + 0.012{y^+}^2} dy^+ + \int_{40}^{y^+} \frac{1}{\frac{1}{Pr} + 0.1 + 0.4767y^+} dy^+ \tag{23}$$

with $y^+$ the dimensionless distance from the cylinder walls:

$$y^+ = \frac{u^*_{wall} y}{\nu} \tag{24}$$

The friction velocity at the wall is defined as:

$$u^*_{wall} = C u_w u^* \tag{25}$$

In the multi-zone model proposed, all the terms in Equation (23) are considered. Assuming $Pr = 70$ [58], the expression of $T^+$ as a function of $y^+$ can be written as:

$$T^+(y^+ \leq 40) = 7.42 \times tan^{-1}[0.0037 \times (24y^+ + 25)] - 0.69 \tag{26}$$

$$T^+(y^+ > 40) = 8.98 + 2.098 \times ln(3.34y^+ \times 10^4 + 1 \times 10^5) - 29.74 \tag{27}$$

The inclusion of the $Pr^{-1}$ term for $y^+ \leq 40$ in Equation (23) incorporates the effects of the laminar contribution in the near wall region. This term is neglected in the solution proposed by Han and

Reitz [58], which assumes that the turbulent effect is dominant. The differences are highlighted in Figure 2 and are observed for $y^+ < 15$.

The equation for the dimensionless temperature profile proposed by Han and Reitz [58], which neglects the $Pr^{-1}$ term for $y^+ \leq 40$, is here reported:

$$T^+ = 21ln(y^+) + 2.5 \tag{28}$$

However, the integration of Equation (23) results in the following expression:

$$T^+ = 21ln(y^+) + 1.24 \tag{29}$$

As can be observed in Figure 2, the difference between the dimensionless temperature profile obtained with Equation (28) (dashed line) and the one with Equation (29) (dotted line) is mainly on the initial slope of the profile ($y^+ \leq 15$). The impact of this difference is smaller than the one related to the $Pr^{-1}$ term mentioned above.

It should be noted that these discrepancies do not affect the results significantly when a reasonably small number of zones is adopted (if the number of zones is less than 25, even for the zones close to the wall, $y^+$ is generally well above 15).

$Cu_w$ (Equation (25)) is required in order to define the heat loss intensity for the engine and it is optimized in terms of in-cylinder temperature profiles and heat flux at the walls, using both experiments and/or non-reactive CFD simulations (see paragraph 2.7.3 for a complete description of the tuning procedure).

## *2.5 Residual Burned Gases (RBG)*

The model presented accounts for the residual exhaust gases from previous cycles. These gases contain hot species deriving from the partial or complete combustion (like CO and $CO_2$) that affect the initial temperature and composition of the fresh charge at valve closure.

During the discharge phase, the piston moves from BDC to TDC, while the exhaust valve is open. In this process, the gases exchange heat with the cylinder wall, while the pressure moves from the value reached at BDC ($P_{end}$) towards the atmospheric pressure. Due to the expansion process and assuming an adiabatic polytropic transformation, the temperature of the RBG trapped in the clearance volume becomes:

$$T_{RBG}^{TDC} = T_{end}\left(\frac{P_{end}}{P_{atm}}\right)^{\frac{1-\gamma}{\gamma}} \tag{30}$$

where $\gamma$ is the heat capacity ratio of the mixture. The effective mixture composition at the beginning of the new cycle is obtained from an ideal non-reactive mixing between the RBG and the fresh charge. Due to the effect of the RBG, it is necessary to simulate several cycles to reach steady engine conditions, usually reached in 3-4 cycles.

## *2.6 Crevices*

In the present multi-zone model, engine crevices are simulated as a single fixed-volume and variable-mass zone that mimics piston-ring pack crevice. During the engine cycle, the mass variation inside the crevices is proportional to the pressure difference at the interface:

$$\Delta\dot{m}_{crev} = C_x\sqrt{|P_1 - P_2|} \tag{31}$$

Depending on the sign of $(P_1 - P_2)$, $\Delta\dot{m}_{crev}$ represents a mass flow rate entering or leaving the crevices and affecting several zones. Since the model does not solve the velocity field, the fluxes $\dot{m}_k$ due to this dynamics are function only of the geometry through the weights $w_k$:

$$\dot{m}_k = \dot{m}_{k-1} - w_k\Delta\dot{m}_{crev} \qquad k = 1, \dots, NZ \tag{32}$$

$$w_k = \frac{1}{d_k\sum_{i=1}^{NCR} 1/d_i} \qquad k = 2, \dots, NCR \tag{33}$$

$$w_k = 0 \qquad k = NCR, \dots, NZ \tag{34}$$

where $d_k$ is the zone thickness. $NCR$ is defined as the outmost zone whose distance from the wall is lower than $S_{crev}$:

$$\sum_{k=2}^{NCR} d_k \leq S_{crev} \tag{35}$$

where $S_{crev}$ is the gap of the top land crevice, obtained from the engine geometry. Since zone sizes change during the cycle, the weights $w_k$ are constantly updated. Only the most external zones are generally affected by the resulting mass fluxes.

The parameter $C_x$ depends on system geometry and affects the instantaneous pressure difference between crevices and cylinder. Its value is estimated through a non-reactive CFD simulation by matching the value of $P_1 - P_2$ predicted by the two models during the cycle. Further details are discussed in paragraph 2.7.2.

## *2.7 Model parameters*

The multi-zone model relies on three engine-specific parameters referring to turbulence, crevices, and wall interactions. In the following, the procedure adopted for defining these model parameters will be presented for the Sandia engine.

### 2.7.1 Turbulence ($Cu_z$)

The definition of $Cu_z$ (Equation (21)) focuses on the evolution of the mass distribution (PDF) of argon in a $N_2$/Ar adiabatic CFD simulation, starting from a segregated configuration where an assigned amount of Ar is placed at the center of the domain (Figure 3 panel A). As the piston moves, argon and nitrogen start mixing due to the turbulent mass transfer process (Figure 3 panel B). The value of $Cu_z$ is optimized to reproduce the evolution of argon mass fraction PDF in the multi-zone model

for the same geometry and initial conditions. Figure 3 shows this procedure referring to the Sandia engine [59]. This approach requires a relatively limited computational time: a non-reactive case lasts about one hour on a 2.6 GHz PC with an initial mesh size of 2400 cells (to simulate a slice of 5 degrees).

### 2.7.2 Crevices ($C_x$)

The same CFD simulation used for defining $Cu_z$ allows to estimate parameter $C_x$ (Equation (31)), by matching the value of $P_1 - P_2$. Panel a of Figure 4 shows how $C_x$ affects model predictions, highlighting that higher values allows a faster alignment between the crevice pressure and one of the other zones. For the Sandia engine, $C_x = 1.5 \cdot 10^{-4}$ reasonably reproduces the non-reactive CFD calculation. Since these pressure differences are very small compared to the system pressure (typically less than 1%), Model predictions are only slightly affected by $C_x$ values. Panel b of Figure 4 confirms this, highlighting that crevice mass (normalized with respect to the total in-cylinder mass) scarcely depends on $C_x$ value. Due to its limited impact on the model predictions, a value of $C_x = 1.5 \cdot 10^{-4}$ has been adopted also for other engines discussed in this work, when detailed crevices geometry was not available.

Model capabilities in predicting the crevices dynamics are also tested under reactive conditions by using the CFD simulation performed by Hessel and co-workers [60] on the Sandia HCCI engine fueled with iso-octane (Figure 5). Panel A shows the mass flux at the crevice interface normalized by its peak value. As can be observed, the model is able to reproduce the dynamics of the mass flux at the crevice interface during the entire engine cycle in reactive conditions. Furthermore, panel B confirms the model capabilities in quantitatively predicting the mass trapped in the crevice (here normalized with respect to the total in-cylinder mass).

### 2.7.3 Wall heat transfer ($Cu_w$)

$Cu_w$ (Equation (25)) is required in order to define the heat loss intensity for the engine and it is optimized in terms of in-cylinder temperature profiles and heat flux at the walls, using experiments and/or non-reactive CFD simulation. Referring to the Sandia engine $Cu_w$, is defined through a non-reactive CFD simulation with pure nitrogen. The optimal value obtained is then used in the multi-zone model (together with the previous parameters) to reproduce the axial temperature profiles measured by Dec and Hwang [61]. Figure 6 shows the complete agreement of model predictions and experimental data along the entire distance from mid-plane to the firedeck, highlighting the predictive capability of the model. Thus, either experimental data or CFD simulations can be used to define the optimal value of $Cu_w$.

Figure 7 and Figure 8 further confirm the reliability of this approach by comparing the heat flux on the piston surface for the GM Triptane (Figure 7) and the Fairbanks-Morse (Figure 8) engines at different speeds (Figure 7) and compression ratios (Figure 8) in non-reactive conditions [62]. The multi-zone model predictions (solid line) are compared with experiments (symbols) and with two CFD predictions: one obtained with the wall function of Rakopoulos et al. [62] (dashed lines) and the other with the wall function of Han and Reitz [58] (dashed lines). It is evident that the wall function implemented in the present multi-zone model is generally able to describe very well the effect of different engine geometries and speeds, both in terms of shape and magnitude. The model also captures the increase of heat losses with the engine speed and compression ratio, due to the higher turbulence and temperature inside the engine.

The approach here proposed also prevents discontinuities in the heat flux predictions. Figure 9 shows the total heat flux predicted by this model (dashed lines) with that calculated by Komninos and Kosmadakis [31] (solid lines) for the Perkins engine at different speeds [62]. As can be observed, at about -65° CA, the model of Komninos and Kosmadakis [31] shows a discontinuity (empathized

by the zoom in Figure 9) due to the switch in the law adopted for the heat flux calculation. The CFD data of Figure 9 (symbols) further confirms the satisfactory capability of the wall-function adopted in describing the heat exchanged with the boundaries.

The proposed multi-zone model is predictive, although it requires three engine-specific parameters. They are defined only once for each engine in a reference configuration (freely chosen) and they are valid for the complete range of motoring and firing conditions. Figure 10 confirms this feature by comparing model predictions with experimental pressure and heat release traces obtained from the Sandia engine at different boost pressures. The model correctly predicts engine performances in the entire spectrum of conditions, without any change in model parameters. The entire tuning procedure here described required only two non-reactive CFD simulations, with and without heat losses, performed with the same engine configuration. Nevertheless, when experimental data of in-cylinder temperature profiles or heat flux at the walls are available, the tuning procedure only requires the adiabatic CFD simulation.

Table 1 summarizes the optimal model parameters together with the operative conditions for the HCCI engines investigated in this work, showing how the different cylinder and piston geometries affect model parameters. In particular, these engines are characterized by a wide spectrum of geometries (i.e. the displacement varies from 377 to 981 $cm^3$, as well as the arm ratio from 3.2 to 4.9), with direct impact on the turbulence and heat/mass transfer intensity.

# 3 Kinetic Mechanism

The POLIMI_1412 kinetic mechanism is used in this work. This general detailed kinetic mechanism, consisting of more than 480 species and 19000 reactions, describes the oxidation of hydrocarbons and oxygenated species up to diesel and bio-diesel fuels [63,64]. The C1-C4 core mechanism features a detailed chemistry model whereas a lumped approach is used for the primary

propagation reactions of larger species. This approach enables an accurate description of the complexity of liquid hydrocarbon mixtures and their pyrolysis and oxidation mechanisms using a limited number of chemical species. Moreover, the extensive use of structural analogies and similarities within the different reaction classes, easily allows the extension of the mechanism to new species [65] and new reaction classes [66]. Thermodynamic properties are taken from literature databases [67] or evaluated on the basis of Benson additivity rules [68]. The validation of the mechanism was carried out in a wide range of operating conditions through extensive comparisons with experimental data in well controlled reaction environments (jet stirred reactors, rapid compression machines, shock tubes, flow reactors and so on) [69,70]. The validation process included also bio-fuels (alcohols and methyl-esters [71,72]), and more complex applications, such as auto-ignition experiments of n-heptane droplets in microgravity conditions [73].

Lumped and derived skeletal kinetic mechanisms have been successfully applied to evaluate the auto-ignition propensities of pure components, surrogate mixtures, and real transportation fuels [74]. In previous works [64,75,76] the mechanism has been validated by comparing model predictions with the performances of SI and HCCI engines over a wide set of operating conditions. The complete kinetic mechanism in CHEMKIN format with thermodynamic and transport properties is available on the CRECK Modeling web site [77].

## *3.1 Kinetics tools*

This multi-zone model has been developed using the OpenSMOKE++ libraries [52], which offer the possibility to manage detailed kinetic mechanisms and provide all the tools for an accurate and efficient description of the thermodynamic and transport properties, as well as the reactivity, of the mixture. In order to investigate the chemistry governing the HCCI combustion, the Rate of

Production Analysis (RoPA) and the Sensitivity Analysis (SA) are implemented in the multi-zone model.

RoPA helps identifying the contribution of each reaction to the production or consumption rates of a species. Following the approach described in [78], for each species $i$ and each reaction $j$ a normalized production $C_{ij}^{p}$ and a normalized consumption contribution $C_{ij}^{d}$ are defined. $C_{ij}^{p}$ and $C_{ij}^{d}$ compare the relative importance of each reaction to the production or consumption rates of a species:

$$C_{ij}^{p} = \frac{max\left(v_{ij}^{f} - v_{ij}^{b}, 0\right) r_j}{\sum_{m=1}^{NR} max\left(v_{ij}^{f} - v_{ij}^{b}, 0\right) r_m} \tag{36}$$

$$C_{ij}^{d} = \frac{min\left(v_{ij}^{f} - v_{ij}^{b}, 0\right) r_j}{\sum_{m=1}^{NR} min\left(v_{ij}^{f} - v_{ij}^{b}, 0\right) r_m} \tag{37}$$

where $v_{ij}$ is the stoichiometric coefficient of species $i$ in reaction $j$. $r$ identifies the reaction, while the superscripts $f$ and $b$ stand for forward and backward respectively.

SA allows a quantitative understanding of how different model parameters affect the dependent variables [79,80], and it represents a powerful tool for studying the kinetics of a reactive system. The multi-zone model can be written in the generic form:

$$\boldsymbol{c}\frac{d\boldsymbol{y}}{dt} = \boldsymbol{f}(\boldsymbol{y}, t, \boldsymbol{\alpha}) \tag{38}$$

where the dependence of functions $\boldsymbol{f}$ on both model unknowns $\boldsymbol{y}$ (size $NE$) and parameters $\boldsymbol{\alpha}$ is assumed (size $NP$) is explicitly introduced. $\boldsymbol{c}$ is a vector (size $NE$) whose elements are equal to 1 for differential variables, and zero for the algebraic. The first-order sensitivity coefficient of the variable $i$ with respect to the parameter $j$ is then defined as:

$$s_{ij} = \frac{\partial y_i}{\partial \alpha_j} \tag{39}$$

The raw sensitivity coefficients $s_{ij}$ are then normalized in the form of logarithmic derivatives, in order to make them more useful for analyses and comparisons:

$$\tilde{s}_{ij} = \frac{\partial \ln y_i}{\partial \ln \alpha_j} = \frac{\alpha_j}{y_i} s_{ij} \tag{40}$$

When detailed kinetic mechanisms are used, the number of sensitivity coefficients can be very large. As an example, with 1000 species, 10.000 reactions, and 10 zones the species sensitivity coefficients are $10^9$. By introducing the vector $\boldsymbol{s}_j$:

$$\boldsymbol{s}_j = \left[\frac{\partial y_1}{\partial \alpha_j}, \frac{\partial y_2}{\partial \alpha_j}, \dots, \frac{\partial y_{NE}}{\partial \alpha_j}\right] \tag{41}$$

and by differentiation of Equations (38) with respect to the parameters, sensitivity equations become the following set of $NP$ additional DAE:

$$\begin{cases} \boldsymbol{c}\dfrac{d\boldsymbol{s}_j}{dt} = \mathbf{J}\boldsymbol{s}_j + \dfrac{\partial \mathbf{f}}{\partial \alpha_j} \\ \boldsymbol{s}_j(t_0) = \mathbf{0} \end{cases} \tag{42}$$

where $\mathbf{J}$ is the Jacobian matrix of the original system (Equation (38)). The sensitivity equations are linear in the sensitivity coefficients with the same Jacobian matrix of the original model. For a relatively small set of parameters, the overall system given by the coupling of Equations (38) and (42) can be solved directly. Being the original model system not coupled with the sensitivity equations, when facing with large kinetic mechanism a modified version of the staggered direct method [81,82] can be applied. Figure 11 shows the block-structure of the overall DAE system (Equations (38) and (42)). Together with the original system of $NE$ equations, there are $NP$ independent DAE systems, one for each specific parameter $\alpha_j$.

As usual for very large systems, sensitivity equations are solved sequentially and separately from the model system (Equations (38)), by assuming the time step $\Delta t$ dictated by the original model. Further details on this procedure and approximations are reported in [52].

# 4 Model Results

Data obtained at Drexel University [28] are used to show how the multi-zone model compares with experimental measurements and to investigate the effects of different model parameters on the engine performances (combustion duration, phasing, and speciation). Table 2 shows the engine characteristics. Data were collected in a single cylinder, four stroke, air-cooled engine coupled to a DC dynamometer. The total displacement is 376 $cm^3$, with a bore of 7.62 cm, and a stroke of 8.26 cm. A custom cylinder head developed at Sandia National Laboratories substitutes the original one, in order to insert a fast sampling probe (2 ms) in the cylinder. Hot sample gases are then analyzed by means of two different GCs.

Experiments refer to an air/PRF20 mixture (80% of n-heptane, 20% of iso-octane) at 750 rpm, equivalence ratio 0.5, with intake temperature and pressure of 423 K and 1 atm. As already discussed in paragraph 2.5, the multi-zone model evaluates the amount of RBG and its composition by simulating several engine cycles. Table 3 reports the complete list of initial and boundary conditions.

Figure 12 shows the predicted average temperature and pressure profiles obtained using 15 zones and by assuming a crevice volume equal to 2.8% of the clearance volume. The two profiles clearly show the low temperature ignition around -40° CA, where the system reaches 800 K and ~8 atm, followed at -18° CA by the hot ignition, characterized by a peak temperature of 2000 K and a maximum pressure of 35 atm. Figure 13 highlights the different behavior of the zones during this dynamics. The low (LT) and high (HT) temperature ignitions in the inner (i.e. $15^{th}$) zone take place at around -40° CA and -18° CA, respectively. Because of the instantaneous pressure increase and of diffusion, hot ignition of the core zone rapidly favors a similar behavior in the neighboring zones. This justifies a more delayed LT ignition of the $5^{th}$ zone at around -30° CA and the HT ignition at -16° CA. The low reactivity of the external and crevice zones is also evident. In fact, these zones are not

able to ignite because of the heat lost with the cylinder walls. Obviously, this behavior directly affects the system performances and emissions. Figure 13 shows that the crevice and the external zone are responsible of CO found in the exhausts [83,84].

Figure 14 compares model predictions with measured in-cylinder average concentrations of n-heptane and iso-octane together with major, minor intermediates and final combustion products. Data are shift of 9° CA in order to account for the delay associated with the sampling time. Experimental data confirm that low temperature ignition starts at ~-40° CA, while hot ignition and complete fuel conversion occurs at least 15° CA before the TDC. Model predictions agree well with the experimental data and the overall conversion process takes about 25° CA, with a sharp low temperature reactivity. A general overestimation of intermediate species is observed. Moreover, it is possible to highlight the initial $CO_2$ concentration due to the recycle of burned gases, as well as the residual fuel, CO, and aldehydes in the exhaust gases mainly due to the crevices.

This is confirmed in Figure 15, where the acetaldehyde profiles in different zones are shown. Before hot ignition, low temperature reactions progressively form $CH_3CHO$ in the inner zones and it reaches the crevice due to mass fluxes. During hot ignition, acetaldehyde is completely consumed in the inner zones, but crevices act like a reservoir, retaining fuel and partially oxidized species, which are released with the exhausts during the expansion phase.

Rather than an extended comparison with experimental data, the aim of this work is to highlight the effects of the different model assumptions, as well as to analyze the sensitivity to major model and kinetic parameters. The results of these analyses are shown in the next sessions.

## *4.1 Effect of model assumptions and parametric sensitivity*

### 4.1.1 Number of zones

Figure 16 shows the predicted engine performances by varying the number of uniform zones (crevice volume has been kept fixed). It is possible to observe that 15 zones are sufficient to obtain a solution independent on the number of sub-domains defined, while 1 or 5 zones leads to significant overestimations of temperature and pressure peaks, as well as their rise rate. These results confirm the limits of a single zone approach, which are mainly related to the very fast energy release during the ignition.

Different results are obtained when a non-uniform initialization is adopted. Here, the volume of the external zone is maintained fixed and equal to 6.5% of the total initial volume (i.e. the value of the previously selected 15-zone case). The other zones uniformly distribute the remaining volume, as reported in Table 4.

Figure 17 shows the predicted engine performances and highlights that 8-10 zones are now sufficient to obtain a solution reasonably independent from the number of zones. This is true not only for temperature and pressure profile, but also for the fuel and CO concentrations during the cycle. This result shows that a better characterization of the temperature gradient only where needed allows reducing the computational effort without significantly affecting the combustion behavior.

A single simulation cycle with 15 zones and 100 species lasts ~2 minutes, and ~10 when 60 zones are used, on a modern 2.6 GHz PC.

### 4.1.2 Residual Burned Gases (RBG)

As already mentioned, exhaust gases from previous cycles affect the engine performances during the next cycle. Based on the design of the Drexel engine and the operating conditions, RBG is estimated to be about 7% of the initial mass. This residual gas leads to an increase in the effective initial temperature and a reduction of the initial fuel concentration, as shown in Figure 18. The increase in the initial temperature has a relevant effect on the system reactivity. Low and high temperature ignitions take place 6-8° CA in advance, while the differences of intermediate aldehydes reflect the variation of fuel concentration and ignition timing.

### 4.1.3 Crevices

Figure 19 confirms that crevices have a significant impact on the overall combustion performances. By neglecting them, temperature and pressure peaks increase, because of the higher fuel conversion and the higher mass inside the cylinder. The presence and size of crevices also affects the exhaust gas composition. Residual fuel trapped in the crevices explains the combustion efficiency of about 97% (i.e. n-heptane out/n-heptane in). Similarly, crevices are responsible of about 350 ppm of CO and traces of intermediate combustion products in the exhaust gases.

### 4.1.4 Equivalent wall temperature

In a real engine cycle, every surface inside the cylinder can potentially follow a different temperature history [48]. Moreover, fuel type, stoichiometry, engine speed, compression ratio, and coolant flow largely affect the surface temperature. This complex scenario makes the definition of an equivalent-average wall temperature a difficult task. Under firing conditions, Heywood [48] suggests that typical temperatures for cylinder walls in diesel engines are 400-450 K, being ~400K the colder

cylinder head and 450-500 K the piston head temperature. For a different engine under motoring conditions, Dec and Hwang [61] estimated a mean cylinder wall temperature around 400 K. Lastly, Chang and co-workers [85] measured the time evolution of the wall temperature on the piston surface and 4 mm below in an HCCI engine. They observed that, while the surface temperature slightly varies along the cycle, moving from 400 K to 405 K, the inner part remains nearly isothermal, with a value of ~395 K. All these data suggest that values between 400 K and 500 K can be reasonably adopted as wall temperature, depending on the conditions. Figure 20 shows the impact of varying ±40 K the effective $T_{wall}$. Model predictions indicate a small sensitivity (±2° CA) to wall temperature in these conditions, where the hot ignition is well established before the TDC, similarly to what observed in [86].

### 4.1.5 Initial temperature distribution

Due to exhaust gas recirculation, thermal stratification inside the cylinder or a non-perfect mixing with the fresh charge can be expected. In order to reproduce this phenomenon, the initial temperatures inside the different zones are assigned assuming a normal distribution with maximum temperature variations of ± 20 K and ± 40 K (corresponding to standard deviations of about 3% and 6% [37,61]), with the higher temperature assigned to the core zone. Figure 21 shows the impact of this initialization on the engine performances. The presence of zones with higher initial temperature advances the combustion phasing of ~6-8 ° CA. Species profiles clearly show the effect on the low temperature reactivity, with a more spread and progressive fuel reactivity. Of course, the higher the variance, the more pronounced these effects are.

### 4.1.6 Heat and mass diffusivity

The inclusion of mass and heat exchange between zones improves the description of HCCI combustion, allowing thermal and composition stratification in the charge. In fact, the lack of an external device able to adjust the ignition timing makes stratification very important in controlling the combustion process. Figure 22 compares the importance of heat and mass exchange among different zones, highlighting the dominant role of heat diffusion on engine performances with respect to the mass exchange. Without heat exchange between adjacent zones, ignition takes place 5-6° CA in advance, while, in these conditions, mass diffusion scarcely affects system behavior. The higher temperature and pressure peaks when no heat exchanges among zones are taken into account is justified by the fact that the inner zones are mainly adiabatic, leading the system to an advanced ignition.

Even if exhausts seem not affected by the removal of heat fluxes among zones in these conditions, this is not true when mass fluxes are neglected. The lack of mass exchanges lead to a lower fuel conversion due to a higher fuel concentration in the colder external and crevice zones that are not interested by the ignition. This, leads to higher amounts of CO and intermediate combustion products in the exhaust gases.

## *4.2 Sensitivity analysis to kinetic parameters*

While in the previous section the model sensitivity has been discussed with respect to different assumptions and engine parameters, here the attention is focused on kinetic parameters.

Kinetic sensitivity analysis for this dynamic problem is a very challenging task, not only because of the complexity of the kinetic mechanism, but also for the presence of several zones. Indeed, the dynamic nature of the problem requires the solution of the system (42) at each time step in order to evaluate the time evolution of sensitivity coefficients for each zone.

Always referring to the Drexel engine, Figure 23 shows an example of kinetic sensitivity analysis for performed in the inner zone. It highlights that low temperature reactions are the most sensitive to set both the low (panel A) and the high temperature ignitions (panel B). In particular, the reaction of peroxy-alkyl-hydroperoxy radicals to form keto-hydroperoxides, together with the oxygen additions to the heptyl radicals and the successive isomerization reaction to form the alkyl-hydroperoxide, enhance the system reactivity. On the contrary, the alkyl-hydroperoxide decomposition and the addition of alkyl radicals on oxygen to form n-heptene and $HO_2$ radicals inhibit the system reactivity. At high temperatures, the sensitivity analysis also shows the positive role of hydrogen-peroxide decomposition reaction.

Figure 24 shows the sensitivity analysis for different zones, by comparing the sensitivity coefficient of n-heptane mass fraction with respect to keto-hydroperoxides formation. It highlights how low temperature ignition progressively moves from the inner core to the external zones. Moreover, it confirms the previous findings that the external and the crevice zones are not able to ignite, as already discussed and observed in Figure 15.

Another possible application of this model is to investigate the dynamics of pollutants formation. Sensitivity analysis with respect to acetaldehyde in the inner zone just before the hot ignition confirms consumption dynamics reported in paragraph 4 and Figure 14. Figure 25 highlights the role of H-abstraction reactions (due to OH, $HO_2$ and H radicals) on acetaldehyde depletion. Again, reactions promoting the system reactivity show positive coefficients, together with the direct acetaldehyde formation through the decomposition of the ketohydroperoxide.

It is relevant to observe that encouraging comparisons with experimental data obtained in a wide range of fuel and engine conditions were already discussed by Bissoli [87]. As an example, Figure 26 shows CO and $CO_2$ emissions from the combustion of both neat 1-butanol and 60%/40% n-heptane/1-butanol mixture obtained in a modified CFR engine [88]. The figure highlights the model

capability to reproduce tailpipe emissions in a wide range of compression ratios, as well as to predict the critical compression ratio characterizing the switching from partial to complete combustion.

# 5 Conclusions

The multi-zone model here presented offers a robust and predictive framework to study the chemistry governing the HCCI combustion cycle. The model accounts for heat and mass transfer between zones, and a novel approach allows a better characterization of the near-wall region and of the heat exchange process with the boundaries. This wall-function approach, coupled with a proper turbulence model, gives a reliable description of the mixture stratification during HCCI combustion. The effect of crevices and residual burned gases are taken into account as well, providing the elements for predicting and quantifying pollutants emission. In order to set up an engine simulation, only three engine-specific parameters need to be evaluated from a non-reactive CFD simulation. These engine specific parameters are valid over a wide range of conditions and allow exploring a vast operating space without further adjustments. The capability of handling detailed kinetic mechanisms allows studying low and high temperature ignition, as well as the in-cylinder speciation. Sensitivity and rate of production analyses permit to investigate system reactivity with real engine cases and to understand how different parameters and conditions affect the combustion performances. All these features contribute in making the proposed multi-zone model a useful predictive tool to investigate combustion chemistry in homogeneous compression ignition engines.

Results show the capability of the model to reproduce the HCCI combustion in terms of phasing, combustion duration and speciation. The comparisons presented in the paper demonstrate how the model can reproduce time-resolved measurements of several species inside the cylinder. These

comparisons are also used to highlight the role of different model assumptions and parameters, as well as the effects of crevices and residual burned gases on the combustion performances.

## Acknowledgments

The authors would like to thanks Tommaso Lucchini and the ICE Group of Politecnico di Milano for providing the CFD tools and William J. Pitz for the useful suggestions.

The LLNL contribution to this work was performed under the auspices of the US Department of Energy by Lawrence Livermore National Laboratory under Contract DE- AC52-07NA27344.

# Reference List


[1] Maurya RK, Agarwal AK. Experimental study of combustion and emission characteristics of ethanol fuelled port injected homogeneous charge compression ignition (HCCI) combustion engine. Appl Energy 2011;88:1169-80.

[2] Fathi M, Saray RK, Checkel MD. The influence of Exhaust Gas Recirculation (EGR) on combustion and emissions of n-heptane/natural gas fueled Homogeneous Charge Compression Ignition (HCCI) engines. Appl Energy 2011;88:4719-24.

[3] Dec JE. Advanced compression-ignition engines—understanding the in-cylinder processes. Proceedings of the Combustion Institute 2009;32:2727-42.

[4] Yao M, Zheng Z, Liu H. Progress and recent trends in homogeneous charge compression ignition (HCCI) engines. Progress in Energy and Combustion Science 2009;35:398-437.

[5] Gowthaman S, Sathiyagnanam AP. The effect of exhaust gas recirculation on performance and emission characteristics of HCCI engine. Int J Ambient Energy 2015.

[6] Mack JH, Schuler D, Butt RH, Dibble RW. Experimental investigation of butanol isomer combustion in Homogeneous Charge Compression Ignition (HCCI) engines. Appl Energy 2016;165:612-26.

[7] Szybist JP, Boehman AL, Haworth DC, Koga H. Premixed ignition behavior of alternative diesel fuel-relevant compounds in a motored engine experiment. Combust Flame 2007;149:112-28.

[8] Yang Y, Boehman AL. Oxidation chemistry of cyclic hydrocarbons in a motored engine: Methylcyclopentane, tetralin, and decalin. Combust Flame 2010;157:495-505.

[9] Dec JE, Yang Y. Boosted hcci for high power without engine knock and with ultra-low nox emissions - using conventional gasoline. SAE Int J Engines 2010;3:750-67.

[10] Sarathy SM, Vranckx S, Yasunaga K, Mehl M, Oßwald P, Metcalfe WK et al. A comprehensive chemical kinetic combustion model for the four butanol isomers. Combust Flame 2012;159:2028-55.

[11] Contino F, Foucher F, Dagaut P, Lucchini T, D'Errico G, Mounaïm-Rousselle C. Experimental and numerical analysis of nitric oxide effect on the ignition of iso-octane in a single cylinder HCCI engine. Combust Flame 2013;160:1476-83.

[12] Vuilleumier D, Kozarac D, Mehl M, Saxena S, Pitz WJ, Dibble RW et al. Intermediate temperature heat release in an HCCI engine fueled by ethanol/n-heptane mixtures: An experimental and modeling study. Combust Flame 2014;161:680-95.

[13] Zheng Z, Lv Z. A new skeletal chemical kinetic model of gasoline surrogate fuel with nitric oxide in HCCI combustion. Appl Energy 2015;147:59-66.

[14] Najt PM, Foster DE. Compression ignited homogeneous charge combustion. SAE Paper 83-0264 1983.

[15] Aceves SM, Smith JR, Westbrook CK, Pitz WJ. Compression ratio effect on methane HCCI combustion. Journal of Engineering for Gas Turbines and Power 1999;121:569-74.

[16] Fiveland SB, Assanis DN. A four-stroke homogeneous charge compression ignition engine simulation for combustion and performance studies. SAE Paper 2000-01-0332 2000.

[17] Woschni G. A Universally Applicable Equation for the Instantaneous Heat Transfer Coefficient in the Internal Combustion Engine. SAE Paper 1967;670931.

[18] Annand W. Heat transfer in the cylinders of reciprocating internal combustion engines. Proceedings of the Institution of Mechanical Engineers 1963;177:973-96.

[19] Hohenberg GF. Advanced approaches for heat transfer calculations. SAE Technical Papers 1979.

[20] Andreatta DA. The use of reformed natural gas as a fuel for reciprocating engines. PhD Dissertation 2000.

[21] Easley WL, Agarwal A, Lavoie GA. Modeling of HCCI combustion and emissions using detailed chemistry. SAE Paper 2001-01-1029 2001.

[22] Noda T, Foster DE. A numerical study to control combustion duration of hydrogen-fueled HCCI by using multi-zone chemical kinetics simulation. SAE Technical Papers 2001.

[23] Fiveland SB, Assanis DN. Development of a two-zone HCCI combustion model accounting for boundary layer effects. SAE Paper 2001-01-1028 2001.

[24] Ogink R, Golovitchev V. Gasoline HCCI modeling: an engine cycle simulation code with a multi-zone combustion model. SAE Paper 2002-01-1745 2002.

[25] Xu H, Liu M, Gharahbaghi S, Richardson S, Wyszynski M, Megaritis T. Modelling of HCCI engines: Comparison of single-zone, multi-zone and test data. SAE Technical Papers 2005.

[26] Orlandini I, Kulzer A, Weberbauer F, Rauscher M. Simulation of self ignition in HCCI and partial HCCI engines using a reduced order model. SAE Paper 2005.

[27] Kodavasal J, McNenly MJ, Babajimopoulos A, Aceves SM, Assanis DN, Havstad MA et al. An accelerated multi-zone model for engine cycle simulation of homogeneous charge compression ignition combustion. International Journal of Engine Research 2013;14:416-33.

[28] Mehl M, Faravelli T, Ranzi E, Miller D, Cernansky N. Experimental and kinetic modeling study of the effect of fuel composition in HCCI engines. Proceedings of the Combustion Institute 2009;32 II:2843-50.

[29] Kozarac D, Lulic Z, Sagi G. A six-zone simulation model for HCCI engines with a non-segregated solver of zone state. Combust Theory Model 2010;14:425-51.

[30] Komninos NP, Hountalas DT, Kouremenos DA. Development of a new multi-zone model for the description of physical processes in HCCI engines. SAE Paper 2004-01-0562 2004.

[31] Komninos NP, Kosmadakis GM. Heat transfer in HCCI multi-zone modeling: Validation of a new wall heat flux correlation under motoring conditions. Appl Energy 2011;88:1635-48.

[32] Kongsereeparp P, Checkel D. Novel method of setting initial conditions for multi-zone HCCI combustion modeling. SAE Paper 2007-01-0674 2007.

[33] Guo H, Li H, Neill WS. A study on the performance of combustion in a HCCI engine using N-heptane by a multi-zone model. Proceedings of the ASME Internal Combustion Engine Division Fall Technical Conference 2009 2010:489-97.

[34] Kraft M, Maigaard P, Mauss F, Christensen M, Johansson B. Investigation of combustion emissions in a homogeneous charge compression injection engine: Measurements and a new computational model. Symp Int Combust 2000;28:1195-201.

[35] Maigaard P, Mauss F, Kraft M. Homogeneous charge compression ignition engine: A simulation study on the effects of inhomogeneities. Journal of Engineering for Gas Turbines and Power 2003;125:466-71.

[36] Pitsch H, Chen M, Peters N. Unsteady flamelet modeling of turbulent hydrogen-air diffusion flames. Symp Int Combust 1998;1:1057-64.

[37] Aceves SM, Flowers DL, Westbrook CK, Smith JR, Pitz W, Robert Dibble R et al. A Multi-Zone Model for Prediction of HCCI Combustion and Emissions. SAE Paper 2000-01-0327 2000.

[38] Aceves SM, Flowers DL, Martinez-Frias J, Smith JR, Westbrook CK, Pitz WJ et al. A sequential fluid-mechanic chemical-kinetic model of propane HCCI combustion. SAE Techni Paper 2001.

[39] Aceves SM, Martinez-Frias J, Flowers DL, Smith JR, Dibble RW, Wright JF et al. A decoupled model of detailed fluid mechanics followed by detailed chemical kinetics for prediction of iso-octane HCCI combustion. SAE Paper 2001-01-3612 2001.

[40] Babajimopoulos A, Assanis DN, Flowers DL, Aceves SM, Hessel RP. A fully coupled computational fluid dynamics and multi-zone model with detailed chemical kinetics for the simulation of premixed charge compression ignition engines. International Journal of Engine Research 2005;6:497-512.

[41] Flowers DL, Aceves SM, Martinez-Frias J, Hessel RP, Dibble RW. Effect of mixing on hydrocarbon and carbon monoxide emissions prediction for isooctane HCCI engine combustion using a multi-zone detailed kinetics solver. SAE Technical Paper 2003.

[42] Shi Y, Hessel RP, Reitz RD. An adaptive multi-grid chemistry (AMC) model for efficient simulation of HCCI and DI engine combustion. Combustion Theory and Modelling 2009;13:83-104.

[43] Felsch C, Hoffmann K, Vanegas A, Drews P, Barths H, Abel D et al. Combustion model reduction for diesel engine control design. International Journal of Engine Research 2009;10:359-87.

[44] Kodavasal J, Keum SH, Babajimopoulos A. An extended multi-zone combustion model for PCI simulation. Combustion Theory and Modelling 2011;15:893-910.

[45] Felsch C, Gauding M, Hasse C, Vogel S, Peters N. An extended flamelet model for multiple injections in di Diesel engines. Proc Combust Inst 2009;32 II:2775-83.

[46] Soyhan HS, Yasar H, Walmsley H, Head B, Kalghatgi GT, Sorusbay C. Evaluation of heat transfer correlations for HCCI engine modeling. Appl Therm Eng 2009;29:541-9.

[47] Bissoli M, Cuoci A, Frassoldati A, Faravelli T, Ranzi E, Lucchini T et al. Detailed Kinetic Analysis of HCCI Combustion Using a New Multi-Zone Model and CFD Simulations. SAE International Journal of Engines 2013;6:1594-609.

[48] Heywood JB. Internal Combustion Engine Fundamentals. : McGraw-Hill, 1988.

[49] R. BB, Warren E. S, Edwin N. L. Transport Phenomena. : Wiley, 2007.

[50] Mathur S, Tondon PK, Saxena SC. Thermal conductivity of binary, ternary and quaternary mixtures of rare gases. Mol Phys 1967;12:569-79.

[51] Zhen J. The potential of using natural gas in HCCI engines: results from zero- and multi-dimensional simulations (Ph.D. Thesis). 2012.

[52] Cuoci A, Frassoldati A, Faravelli T, Ranzi E. OpenSMOKE++: An object-oriented framework for the numerical modeling of reactive systems with detailed kinetic mechanisms. Comput Phys Commun 2015;192:237-64.

[53] Hindmarsh AC, Brown PN, Grant KE, Lee SL, Serban R, Shumaker DE et al. SUNDIALS: Suite of nonlinear and differential/algebraic equation solvers. ACM Transactions on Mathematical Software 2005;31:363-96.

[54] Yang J, Martin JK. Approximate solution - one-dimensional energy equation for transient, compressible, low Mach number turbulent boundary layer flows. Journal of Heat Transfer 1989;111:619-24.

[55] Reichardt H. Vollständige Darstellung der turbulenten Geschwindigkeitsverteilung in glatten Leitungen. ZAMM-Journal of Applied Mathematics and Mechanics/Zeitschrift für Angewandte Mathematik und Mechanik 1951;31:208-19.

[56] Herring HJ, Mellor GL. A method of calculating compressible turbulent boundary layers. National Aeronautics and Space Administration 1968.

[57] Lucchini T, D'Errico G, Ettorre D, Brusiani F, Bianchi GM, Montanaro A et al. Experimental and numerical investigation of high-pressure diesel sprays with multiple injections at engine conditions. SAE Techni Paper 2010:321-33.

[58] Han Z, Reitz RD. A temperature wall function formulation for variable-density turbulent flows with application to engine convective heat transfer modeling. Int J Heat Mass Transfer 1997;40:613-25.

[59] Dronniou N, Dec J. Investigating the development of thermal stratification from the near-wall regions to the bulk-gas in an HCCI engine with planar imaging thermometry. SAE Technical Papers 2012.

[60] Hessel RP, Foster DE, Aceves SM, Lee Davisson M, Espinosa-Loza F, Flowers DL et al. Modeling Iso-octane HCCI using CFD with multi-zone detailed chemistry; Comparison to detailed speciation data over a range of lean equivalence ratios. SAE Technical Papers 2008.

[61] Dec JE, Hwang W. Characterizing the development of thermal stratification in an HCCI engine using planar-imaging thermometry. SAE International Journal of Engines 2009;2:421-38.

[62] Rakopoulos CD, Kosmadakis GM, Pariotis EG. Critical evaluation of current heat transfer models used in CFD in-cylinder engine simulations and establishment of a comprehensive wall-function formulation. Appl Energy 2010;87:1612-30.

[63] Ranzi E, Frassoldati A, Grana R, Cuoci A, Faravelli T, Kelley AP et al. Hierarchical and comparative kinetic modeling of laminar flame speeds of hydrocarbon and oxygenated fuels. Progress in Energy and Combustion Science 2012;38:468-501.

[64] Bissoli M, Frassoldati A, Cuoci A, Faravelli T, Ranzi E. Kinetic Modeling of the Low Temperature Reactivity of N-Butanol. XXXVI Meeting of the Italian Section of the Combustion Institute 2013.

[65] Dagaut P, Ristori A, Frassoldati A, Faravelli T, Dayma G, Ranzi E. Experimental and semi-detailed kinetic modeling study of decalin oxidation and pyrolysis over a wide range of conditions. Proceedings of the Combustion Institute 2013;34:289-96.

[66] Pelucchi M, Bissoli M, Cavallotti C, Cuoci A, Faravelli T, Frassoldati A et al. Improved kinetic model of the low-temperature oxidation of n-heptane. Energy Fuels 2014;28:7178-93.

[67] Kee RJ, Rupley F, Miller JA. Sandia Report SAND89-8009. Sandia National Laboratories 1989.

[68] Benson SW. Thermochemical Kinetics. New York: Wiley, 1976.

[69] Van Geem KM, Cuoci A, Frassoldati A, Pyl SP, Marin GB, Ranzi E. An experimental and kinetic modeling study of pyrolysis and combustion of acetone-butanol-ethanol (ABE) mixtures. Combustion Sci Technol 2012;184:942-55.

[70] Frassoldati A, Grana R, Faravelli T, Ranzi E, Oßwald P, Kohse-Höinghaus K. Detailed kinetic modeling of the combustion of the four butanol isomers in premixed low-pressure flames. Combust Flame 2012;159:2295-311.

[71] Grana R, Frassoldati A, Faravelli T, Niemann U, Ranzi E, Seiser R et al. An experimental and kinetic modeling study of combustion of isomers of butanol. Combust Flame 2010;157:2137-54.

[72] Saggese C, Frassoldati A, Cuoci A, Faravelli T, Ranzi E. A lumped approach to the kinetic modeling of pyrolysis and combustion of biodiesel fuels. Proceedings of the Combustion Institute 2013;34:427-34.

[73] Cuoci A, Frassoldati A, Faravelli T, Ranzi E. Numerical modeling of auto-ignition of isolated fuel droplets in microgravity. Proc Combust Inst 2015;35:1621-7.

[74] Ranzi E, Frassoldati A, Stagni A, Pelucchi M, Cuoci A, Faravelli T. Reduced kinetic schemes of complex reaction systems: Fossil and biomass-derived transportation fuels. Int J Chem Kinet 2014;46:512-42.

[75] Mehl M, Faravelli T, Ranzzi E, Lucchini T, Onorati A, Giavazzi F et al. Kinetic Modeling of Knock Properties in Internal Combustion Engines. SAE Paper 2006-01-3239 2006.

[76] Mehl M, Tardani A, Faravelli T, Ranzi E, D'Errico G, Lucchini T et al. A Multizone approach to the detailed kinetic modeling of HCCI combustion. SAE Paper 2007-24-0086 2007.

[77] CRECK Modeling Group. http://creckmodeling.chem.polimi.it/.

[78] Kee RJ, Rupley FM, Meeks E, Miller JA. CHEMKIN-III: A FORTRAN chemical kinetics package for the analysis of gas-phase chemical and plasma kinetics. : Sandia National Laboratories Livermore, CA, 1996.

[79] Miller JA, Branch MC, McLean WJ, Chandler DW, Smooke MD, Kee RJ. The conversion of HCN to NO and N2 in H2-O2-HCN-Ar flames at low pressure. Symp Int Combust 1985;20:673-84.

[80] Lutz AE, Kee RJ, Miller JA. SENKIN: A FORTRAN program for predicting homogeneous gas phase chemical kinetics with sensitivity analysis. Sandia National Laboratories Report SAND87-8248 1988.

[81] Rabitz H, Kramer M, Dacol D. Sensitivity analysis in chemical kinetics. Annu Rev Phys Chem 1983;34:419-61.

[82] Caracotsios M, Stewart WE. Sensitivity analysis of initial value problems with mixed ODEs and algebraic equations. Comput Chem Eng 1985;9:359-65.

[83] Christensen M, Johansson B, Hultqvist A. The effect of piston topland geometry on emissions of unburned hydrocarbons from a Homogeneous Charge Compression Ignition (HCCI) engine. SAE Techni Paper 2001.

[84] Aceves SM, Flowers DL, Espinosa-Loza F, Martinez-Frias J, Dibble RW, Christensen M et al. Piston-liner crevice geometry effect on HCCI combustion by multi-zone analysis. SAE Techni Paper 2002.

[85] Chang J, Güralp O, Filipi Z, Assanis D, Kuo TW, Najt P et al. New heat transfer correlation for an HCCI engine derived from measurements of instantaneous surface heat flux. SAE Technical Papers 2004.

[86] Komninos NP. The effect of thermal stratification on HCCI combustion: A numerical investigation. Appl Energy 2015;139:291-302.

[87] Bissoli M. Multi-Zone Model for HCCI Combustion (Ph.D. Thesis). 2016.

[88] Zhang Y, Boehman AL. Oxidation of 1-butanol and a mixture of n-heptane/1-butanol in a motored engine. Combust Flame 2010;157:1816-24.

[89] Yang J, Pierce P, Martin JK, Foster DE. Heat transfer predictions and experiments in a motored engine. SAE Techni Paper 1988.

[90] Lawton B. Effect of compression and expansion on instantaneous heat transfer in reciprocating internal combustion engines. Proc Inst Mech Eng Part A 1987;20 l:l75-186.

# List of Tables

| Engine | RPM | CR | Displacement [$cm^3$] | $Cu_z$ | $Cu_w$ |
|---|---|---|---|---|---|
| **Fairbanks-Morse [89,90]** | 900 | 8-14 | 503 | 0.06 | 0.3 |
| **GM Triptane [89,90]** | 750-1500 | 9 | 420 | 0.24 | 0.5 |
| **Perkins [31]** | 705-2400 | 16 | 965 | 0.06 | 0.7 |
| **Sandia [9]** | 1200 | 14 | 981 | 0.10 | 0.7 |
| **Drexel [28]** | 750 | 8.2 | 377 | 0.03 | 0.83 |
| **CRF [88]** | 600-900 | 4.5-13 | 613 | 0.09 | 0.56 |

*Table 1: Operating conditions of tested HCCI engines and optimal engine-specific parameters.*

| | |
|---|---|
| Displacement [$cm^3$] | 377.69 |
| Bore [mm] | 76.2 |
| Stroke [mm] | 82.6 |
| Compression Ratio [-] | 8.2 |
| Speed [RPM] | 750 |
| Intake Valve Closing [°BTDC] | 155 |
| Exhaust Valve Opening [°ATDC] | 153 |

*Table 2: Characteristics of Drexel engine [28].*

| Fuel | PRF20 |
|---|---|
| Equivalence Ratio [-] | 0.5 |
| Temperature [K] | 423 |
| Pressure [atm] | 1 |
| Twall [K] | 450 |

*Table 3: Operating conditions for Drexel engine [28].*

| **Total Zone number** | 5 | 8 | 10 | 12 |
|---|---|---|---|---|
| **Crevices [%]** | 0.10 | 0.10 | 0.10 | 0.10 |
| **External zone [%]** | 6.5 | 6.5 | 6.5 | 6.5 |
| **All other zones [%]** | 31.13 | 15.57 | 11.68 | 7.18 |

*Table 4: Initial volume distribution for the case shown in Figure 17.*

# List of Figures

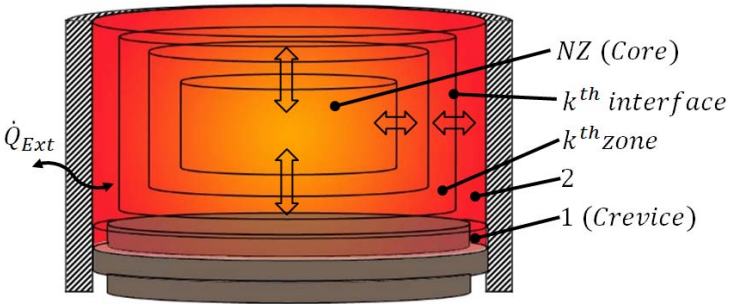


*Figure 1: Zone configuration adopted in the present model.*

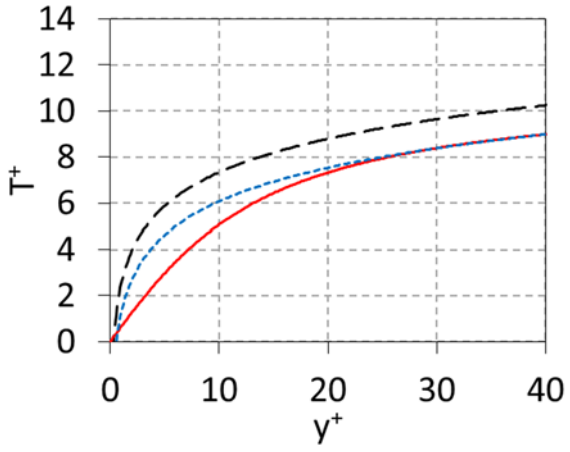


*Figure 2: Dimensionless temperature profiles as a function of dimensionless wall distance. Comparison among Equation (26) (red solid line), (28) (black dashed line), and (29) (blue dotted line).*

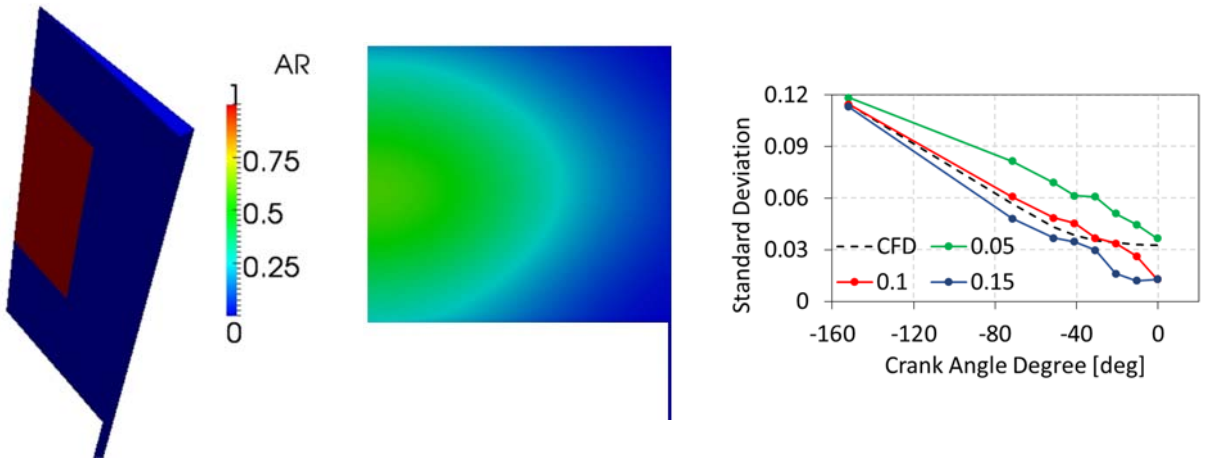


a) b) c)

*Figure 3: Sandia engine, motoring conditions. Argon mass fraction PDF evolution in the CFD simulation. Panel a: -158° CA (initial condition). Panel b: -66.5° CA. Mesh is a 5° slice. Panel c: standard deviation of argon mass fraction PDF along the CAD for different $Cu_z$ parameters. Dashed line: CFD simulation.*

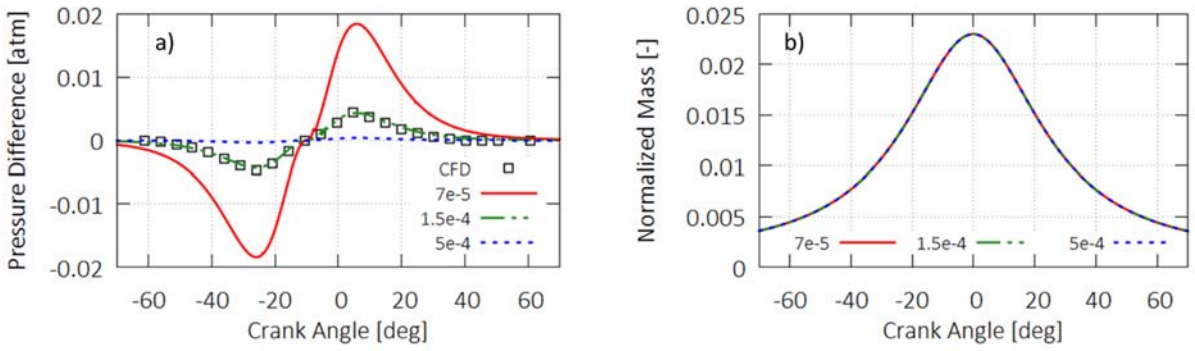


*Figure 4: Sandia engine, motoring conditions. Effect of parameter $C_x$ on the pressure difference between the crevices and the external zone (panel a) and on the mass trapped in the crevices normalized with respect to the total mass (panel b). Symbols: CFD simulation.*

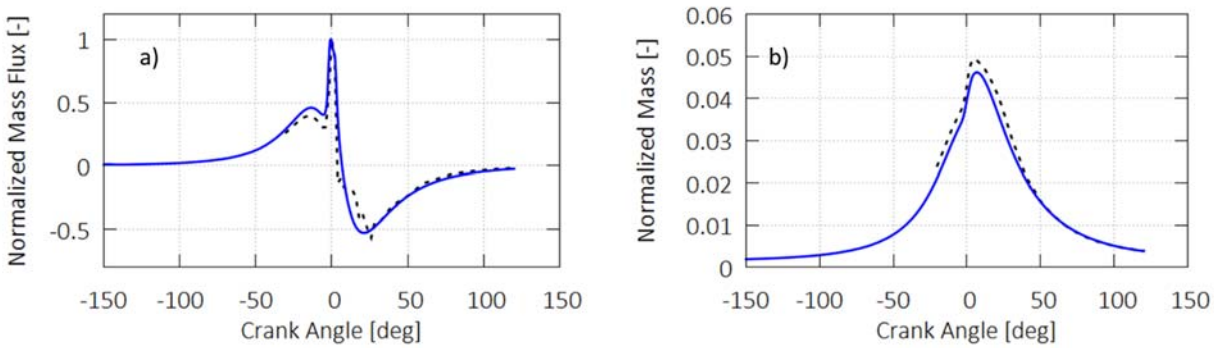


*Figure 5: Sandia engine, iso-octane combustion at 1200 rpm and equivalence ratio 0.20. Normalized mass flux at the crevice interface (panel a) and normalized crevice mass (panel b). Comparison between CFD simulation [60] (dashed lines) and multi-zone model predictions (solid lines). Initial temperature for multi-zone model is 450 K instead of 474 K (CFD) in order to match the combustion phasing.*

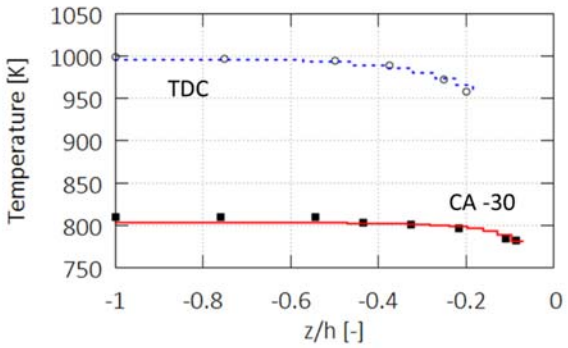


*Figure 6: Sandia engine, motoring conditions. Temperature profiles in the axial direction at two different crank angles. The axial distance –z is normalized by h, the firedeck to mid-plane distance (z/h = -1 is the mid-plane, z/h = 0 is the firedeck). Lines: this multi-zone model. Symbols: experiments [61].*

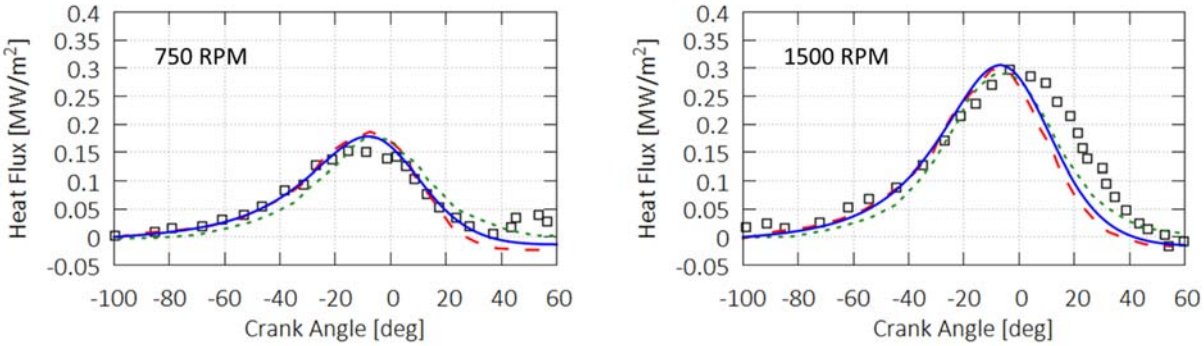


*Figure 7: GM Triptane engine. Heat flux on piston head at two different speeds. Solid lines: this multi-zone model. Dashed lines: CFD with the wall function of Rakopoulos et al. [62]. Dotted lines: CFD with the wall function of Han and Reitz [58]. Symbols: experiments [89,90].*

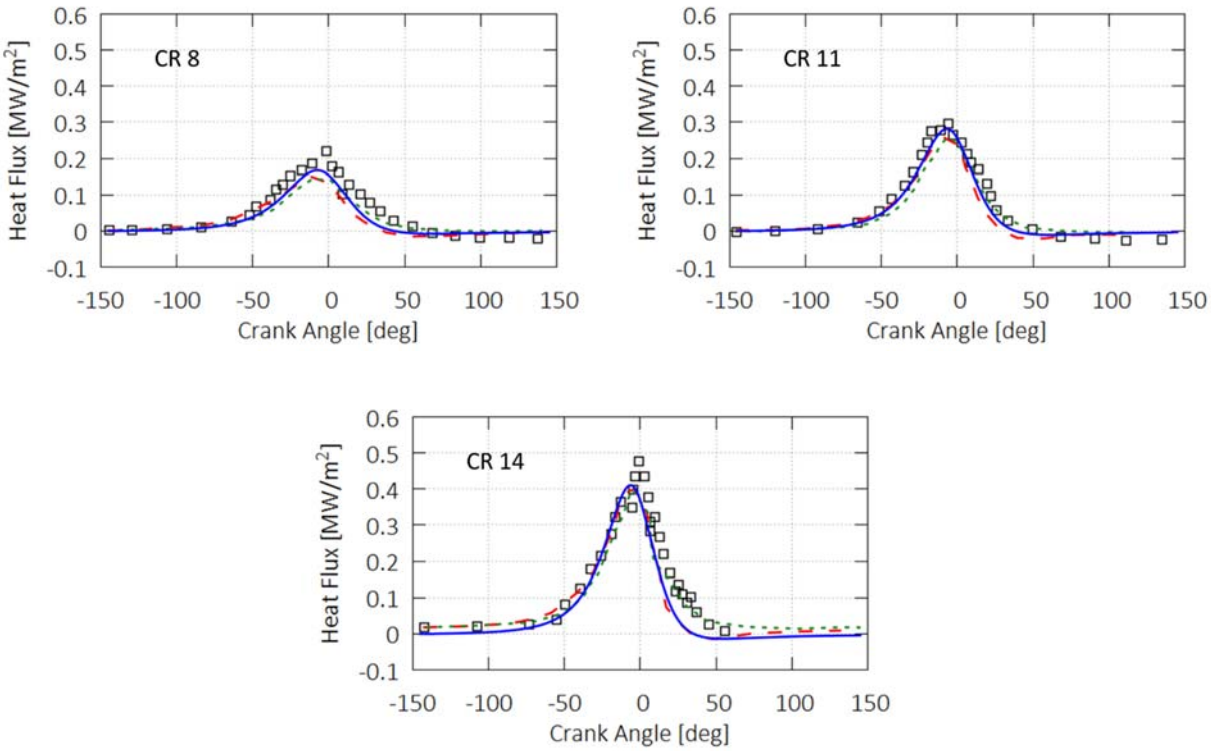


*Figure 8: Fairbanks-Morse engine. Heat flux on piston head at three different compression ratios. Solid lines: this multi-zone model. Dashed lines: CFD with the wall function of Rakopoulos et al. [62]. Dotted lines: CFD with the wall function of Han and Reitz [58]. Symbols: experiments [89,90].*

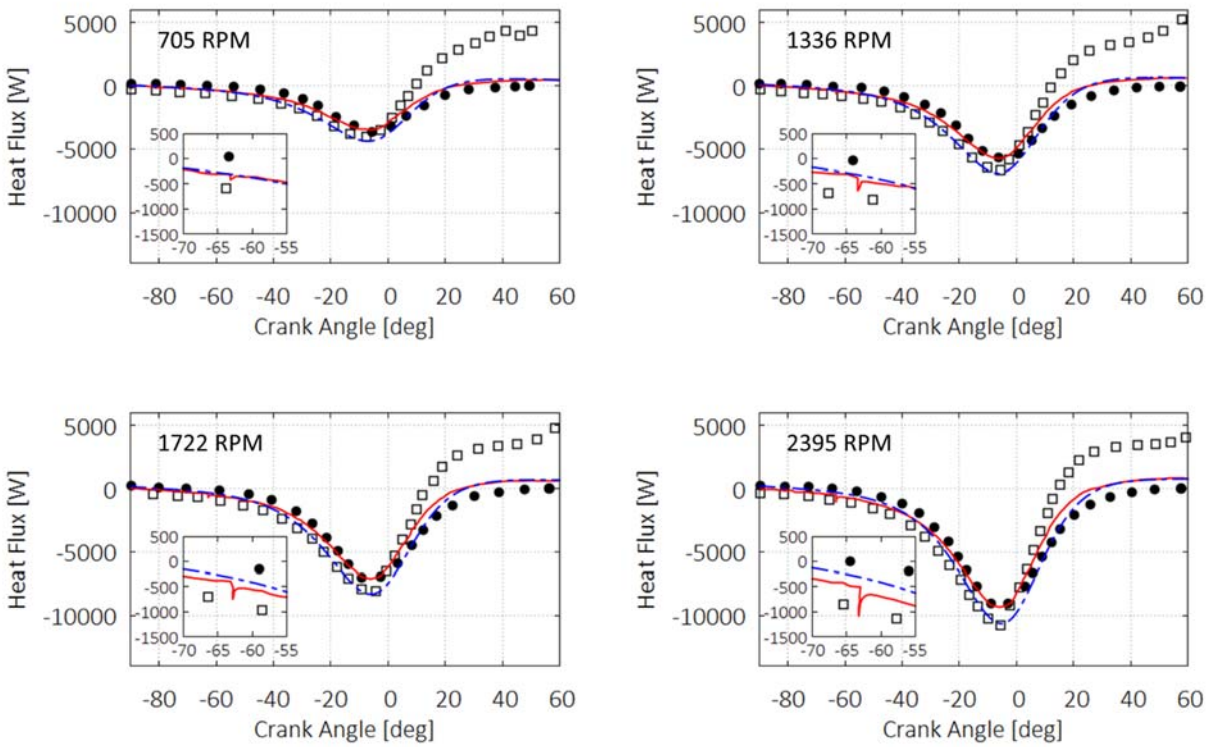


*Figure 9: Perkins engine. Total heat flux at different speeds. Dashed lines: this multi-zone model. Solid lines: multi-zone model of Komninos et al. [31]. Empty symbols: CFD with wall function of Rakopoulos et al. [62]. Full symbols: CFD with wall function of Han and Reitz [58]. Zoom highlights the discontinuity in the model prediction of Komninos et al. [31].*

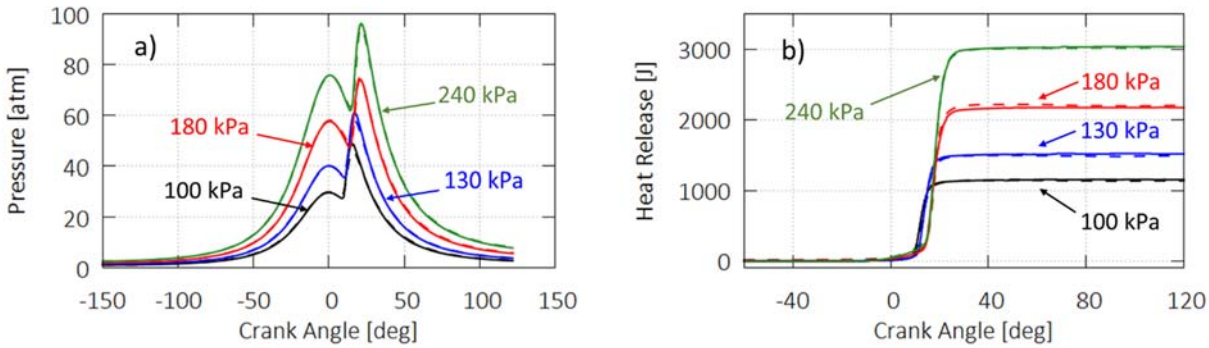


*Figure 10: Sandia engine, gasoline combustion at 1200 rpm. Pressure (panel a) and heat release (panel b) traces at different boost pressures. Comparison between experimental data [9] (dashed lines) and multi-zone model predictions (solid lines) using the parameters defined in this paragraph.*

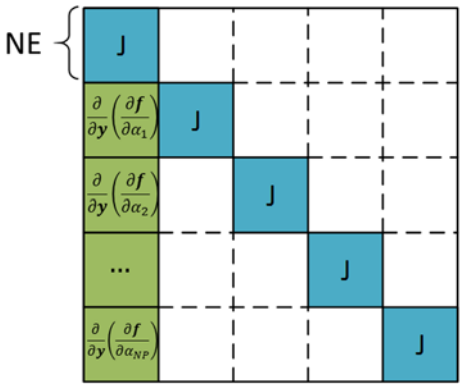


*Figure 11: Sparsity pattern of Jacobian matrix of the whole model and sensitivity equation system. NE is the number of independent variables and NP the number of parameters. Each block is a NE square matrix. The blocks on the main diagonal are equal to the Jacobian matrix J.*

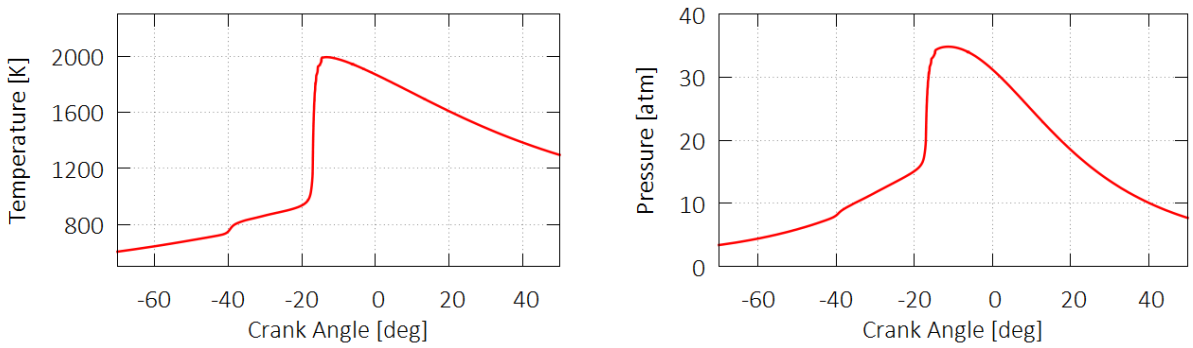


*Figure 12: Drexel engine. PRF20 mixture at 750 rpm and equivalence ratio 0.5. Predicted temperature and pressure profiles.*

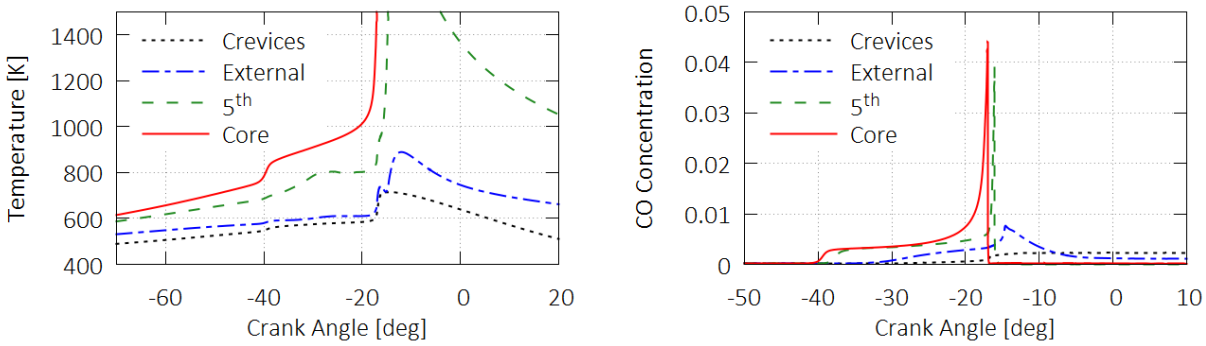


*Figure 13: Drexel engine. PRF20 mixture at 750 rpm, equivalence ratio 0.5. Predicted temperature and CO mole fraction in different zones.*

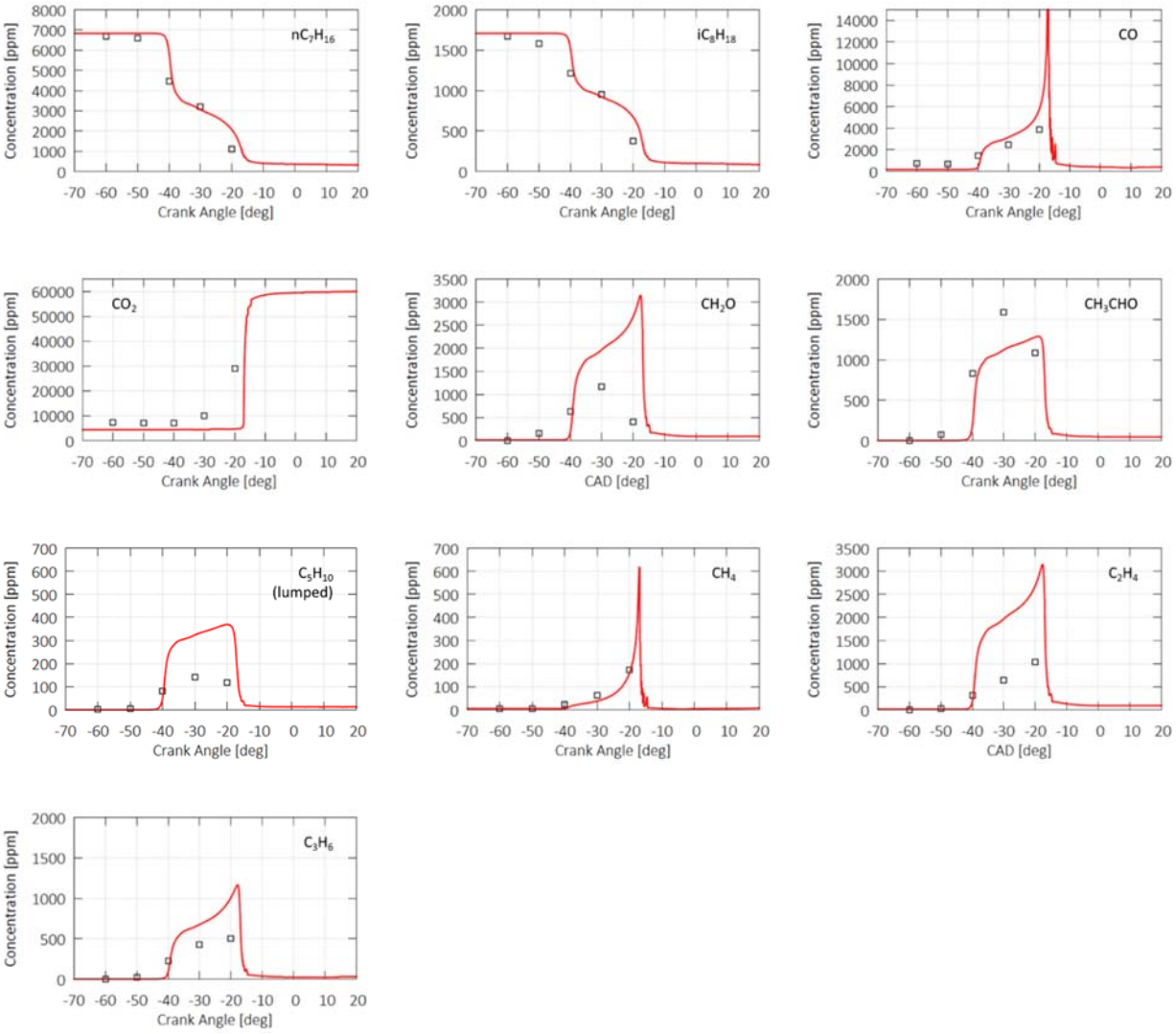


*Figure 14: Drexel engine. PRF20 mixture at 750 rpm, equivalence ratio 0.5. Average in-cylinder species profiles along the engine cycle. Comparison between experiments [28] (symbols) and model predictions (lines).*

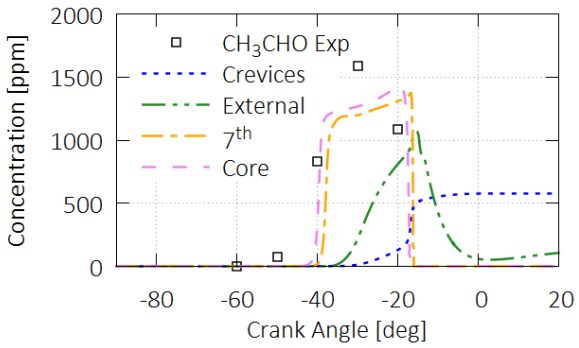


*Figure 15: Drexel engine. PRF20 mixture at 750 rpm, equivalence ratio 0.5. Acetaldehyde profiles in different zones (lines). Symbols: experiments.*

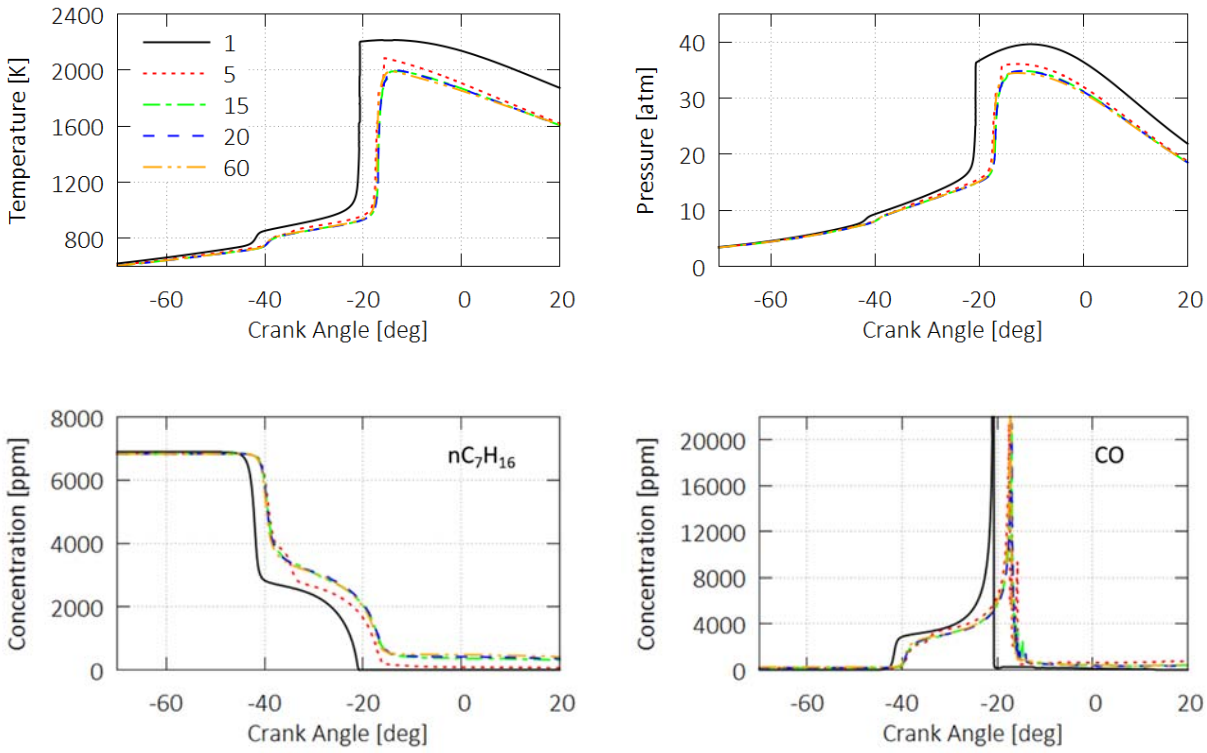


*Figure 16: Drexel engine. Predicted temperature, pressure, and species profiles for different number of zones using a uniform initialization.*

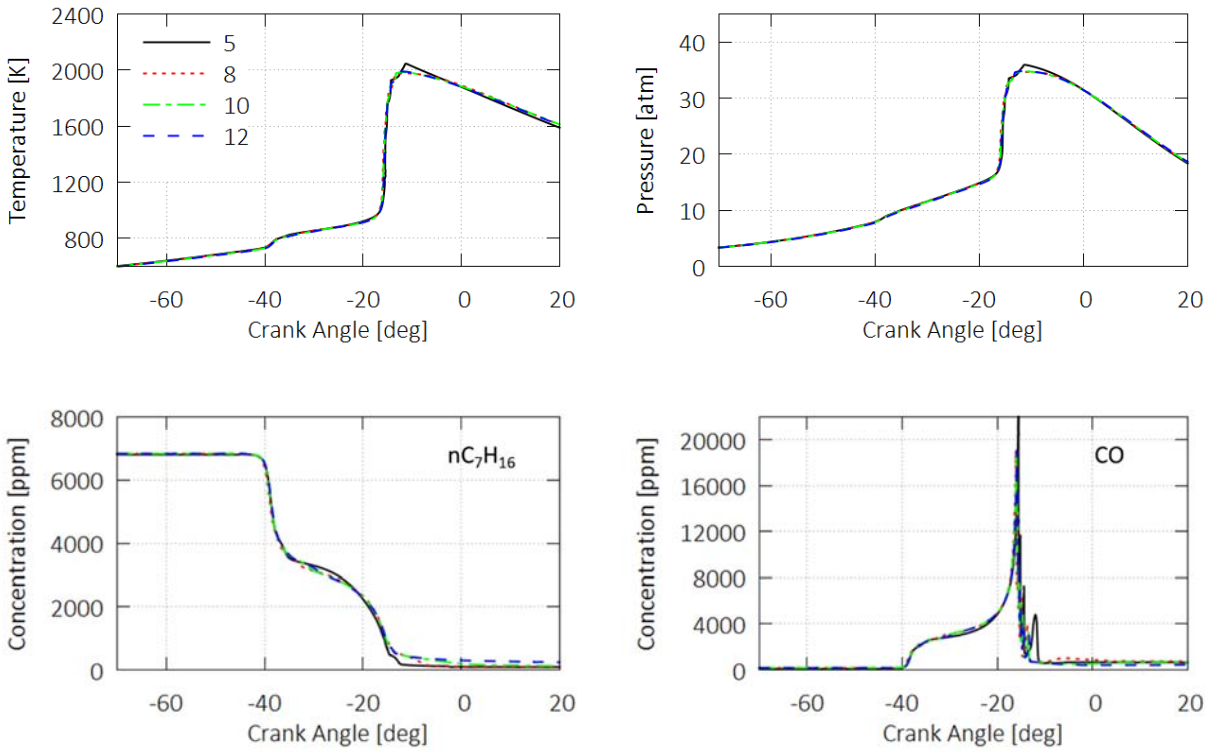


*Figure 17: Drexel engine. Predicted temperature, pressure, and species profiles for different number of zones with fixed dimension of the external zone (see Table 4).*

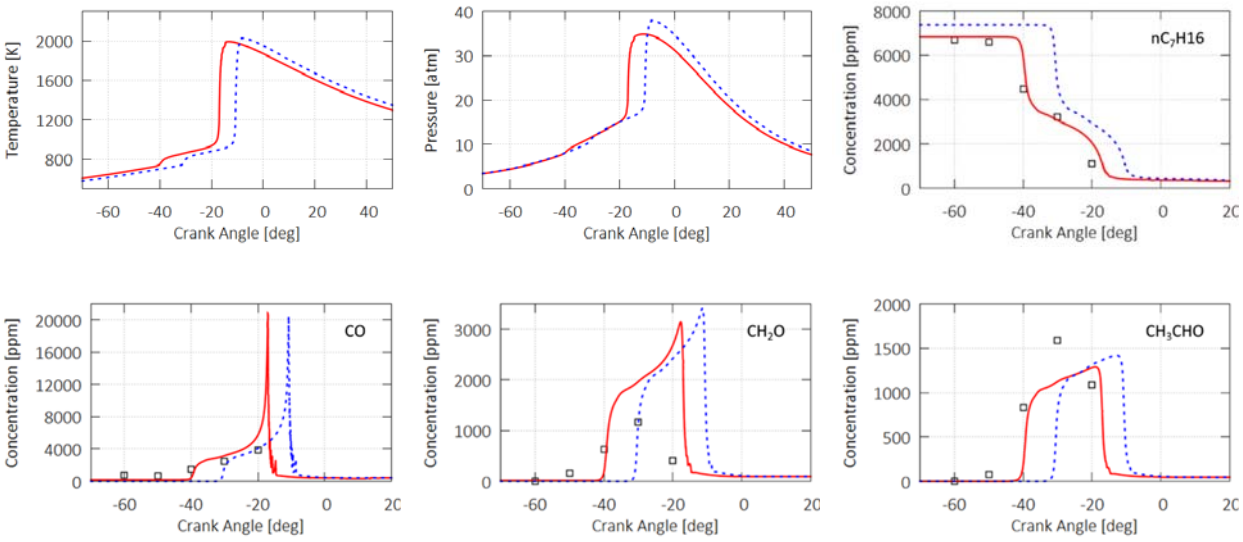


*Figure 18: Drexel engine. Effect of residual burned gases (RBG). Predicted temperature, pressure and species profiles. Symbols: experiments [28]. Solid line: with RBG. Dotted lines: without RBG.*

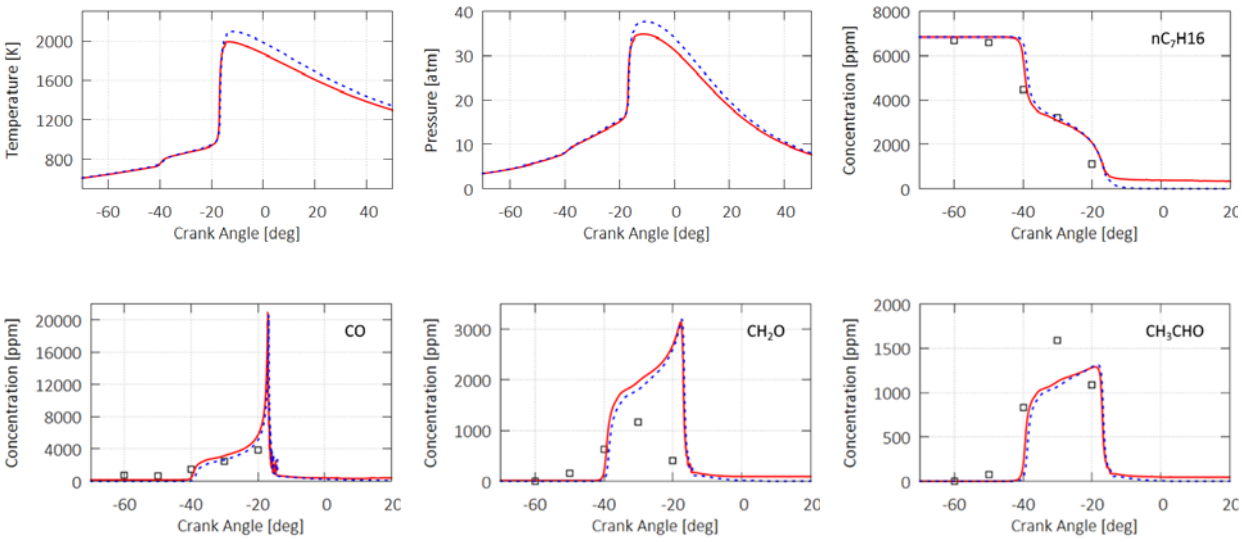


*Figure 19: Drexel engines. Effect of crevices on engine performances. Predicted temperature, pressure and species profiles. Symbols: experiments [28]. Solid line: with crevices. Dotted lines: without crevices.*

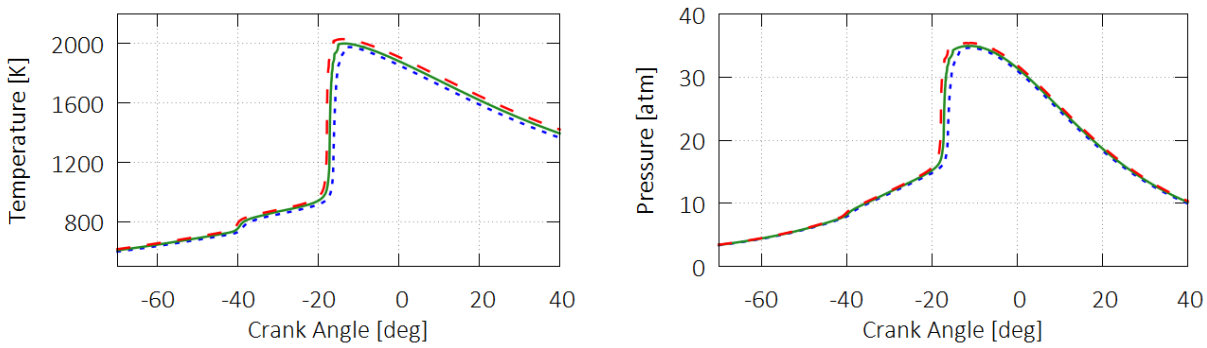


*Figure 20: Drexel engine. Effect of wall temperature. Predicted temperature, pressure and species profiles. Solid line: reference case (450 K). Dotted lines (410 K). Dashed lines (490 K).*

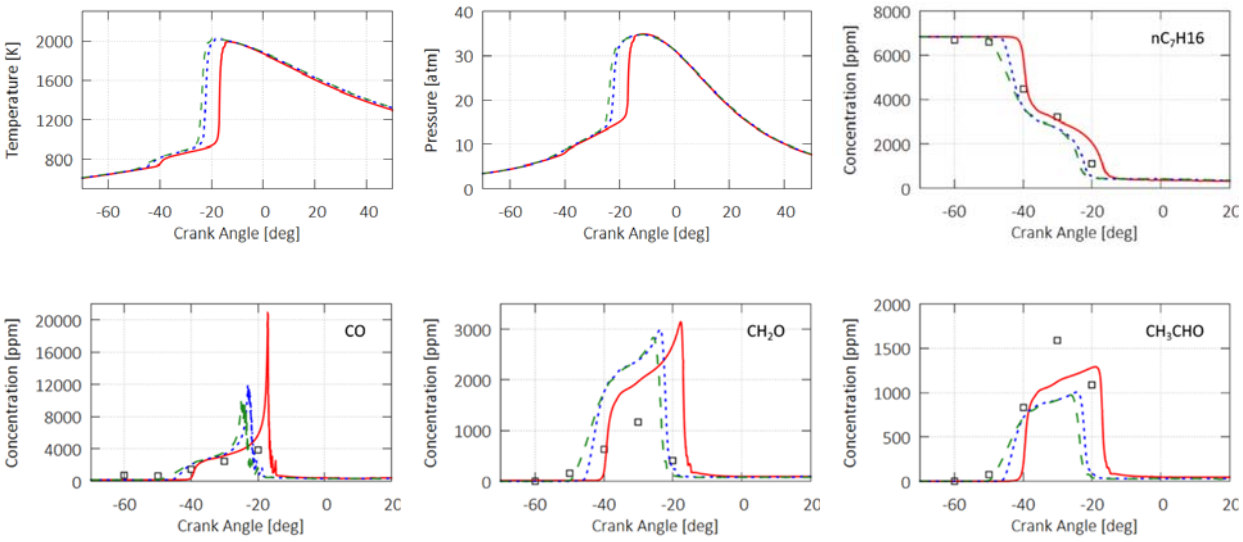


*Figure 21: Drexel engine. Effect of the initial temperature distribution on engine performances. Predicted average temperature, pressure and species profiles. Symbols: experiments [28]. Solid line: uniform temperature distribution. Dotted lines: ±20 K. Dashed line: ±40 K.*

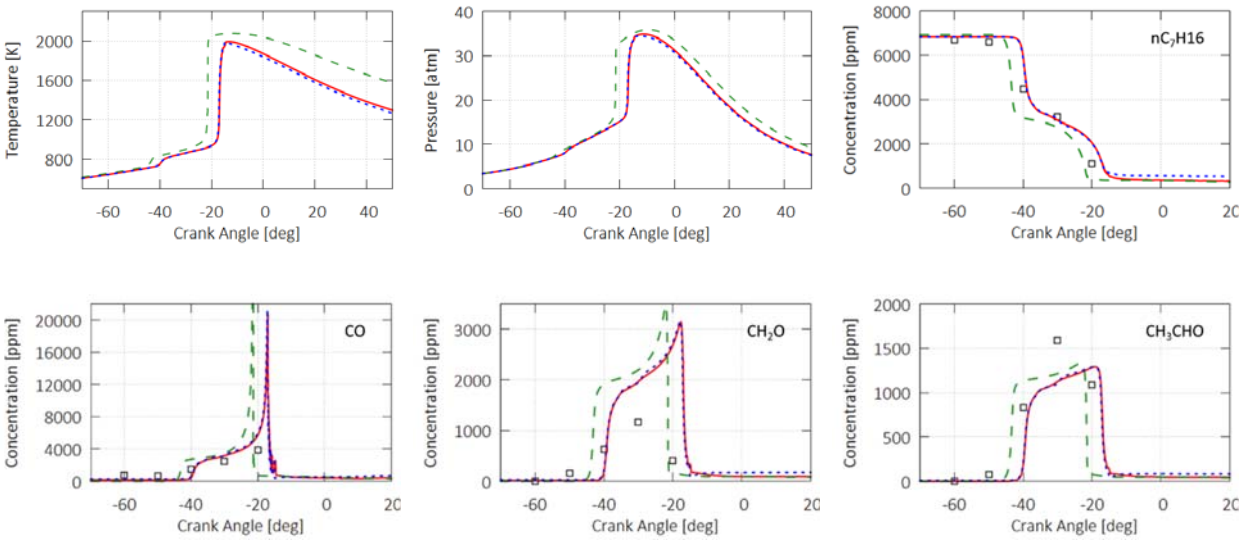


*Figure 22: Drexel engine. Effect of the heat and mass diffusion between zones. Predicted temperature, pressure and species profiles. Symbols: experiments [28]. Solid line: Reference Case; dashed lines: without heat diffusion; dotted lines: without mass diffusion.*

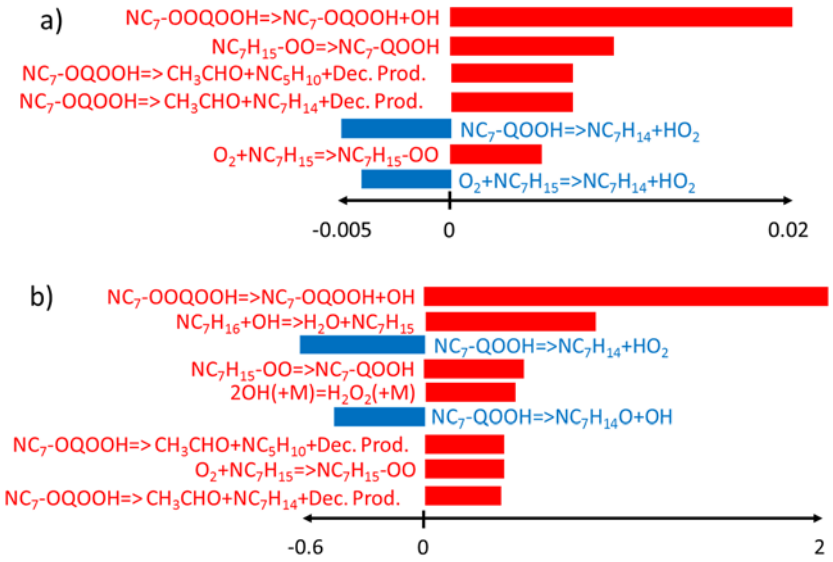


*Figure 23: Sensitivity analysis on temperature in the inner zone at two different CA: -32° (panel a) and -10° (panel b).*

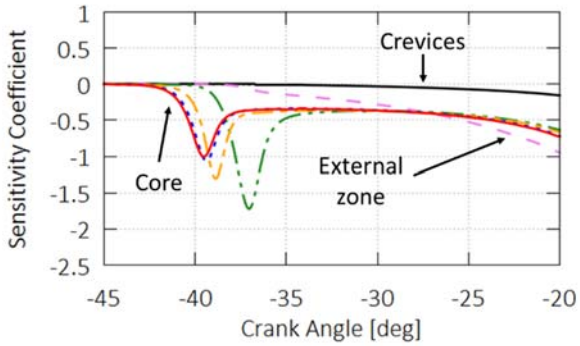


*Figure 24: Sensitivity coefficient of n-heptane mass fraction with respect to keto-hydroperoxides formation in different zones.*

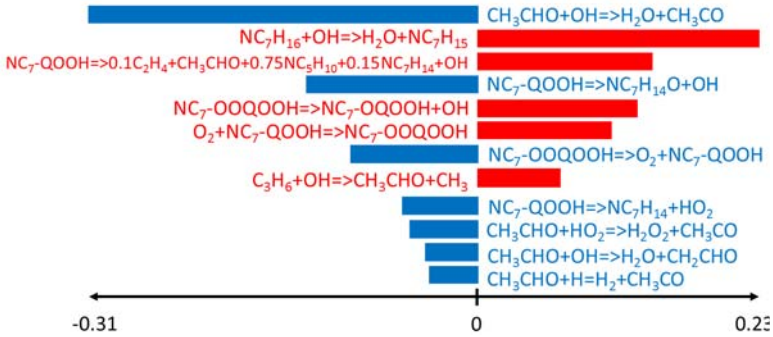


*Figure 25: Sensitivity analysis on acetaldehyde. Inner zone at -10° CA.*

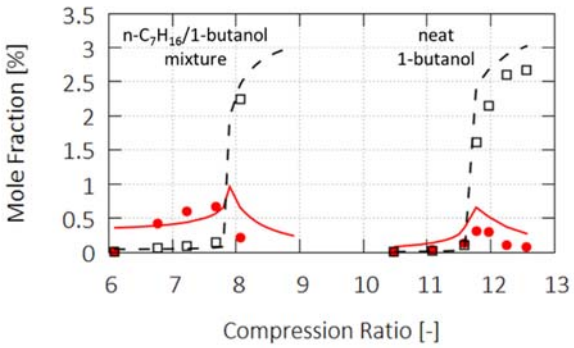


*Figure 26: modified CFR engine, $nC_7H_{16}$/1-butanol (60%/40%) mixture (left side) and neat 1-butanol (right side) combustion at 600 rpm and equivalence ratio 0.25. CO (full and solid) and $CO_2$ (empty and dashed) emissions. Symbols: experiments [88]; lines: multi-zone model predictions.*